MODELING THE CAPILLARY DISCHARGE OF AN ELECTROTHERMAL (ET) LAUNCHER

by

TRAVIS LEAST

Presented to the Faculty of the Graduate School of

The University of Texas at Arlington in Partial Fulfillment

of the Requirements

for the Degree of

MASTER OF ELECTRICAL ENGINEERING

THE UNIVERSITY OF TEXAS AT ARLINGTON

May 2014

Acknowledgements

I would like to begin by thanking Dr. David Wetz for granting me the opportunity to come on his team as one of his research students. I am very grateful for his support, and the lessons learned over the last two years. Without his support I would not have succeeded in my pursuit of higher education. I would like to thank Mr. Doyle Motes for giving help in deciphering the FORTRAN code. Also I would like to thank James Reed, Clint Gnegy-Davidson, and Isaac Cohen for their help with converting FORTRAN to Matlab. And I very much appreciate the help and support given to me by Dr. Wei-Jen Lee. Finally a thanks to my graduate advisors Dr. William Dillon and Dr. Alan Davis for their oversight and guidance.

March 4, 2014

Abstract

Modeling the Capillary Discharge of an Electrothermal (ET) Launcher

Travis Michael Least, MSEE

The University of Texas at Arlington, 2014

Supervising Professor: David Wetz

Over the past few decades, different branches of the US Department of Defense (DoD) have invested at improving the field ability of electromagnetic launchers. One such focus has been on achieving hypervelocity launch velocities in excess of 7 km/s for direct launch to space applications [1]. It has been shown that pre-injection is required for this to be achieved. One method of pre-injection which has promise involves using an electro-thermal (ET) due to its ability to achieve the desired velocities with a minimal amount of hot plasma injected into the launcher behind the projectile. Despite the demonstration of pre-injection using this method, polymer ablation is not very well known and this makes it challenging to predict how the system will behave for a given input of electrical power. In this work, the rate of ablation has been studied and predicted using different models to generate the best possible characteristic curve.

Table of Contents

List of Illustrations

List of Tables

Nomenclature

a	Area
B	Magnetic field
c_p	Specific heat at constant pressure
c_v	Specific heat at constant volume
C	Capacitance
E	Energy
F	Force
f	Adjustment factor
$G_{j\alpha i}$	Degeneracy factor for *jth* energy level in ith ionization of species α
h	Planck's constant
I	Current
$I_{j\alpha}$	*jth* ionization potential of species α
J	Current density
k	Boltzmann's constant
$K_{j\alpha}$	Saha equation fraction for *jth* ionization of species α
L	Inductance
m	Mass
n	Number density
P	Pressure
q	Electric charge
R	Electrical resistance

r_b Capillary radius

t Time

T Bulk gas temperature

T_s Polyethylene surface temperature

$U_{j\alpha i}$ Electronic excitation energy for *jth* energy level in ith ionization of species α

v Velocity

V Voltage

$W_{j\alpha}$ Electronic excitation energy for *ith* ionization of species α

x Time dependant position

x_i Initial position

$x_{j\alpha}$ jth ionization concentration of species α

x_r Reference position

Z Percentage of ionized species

$Z_{j\alpha}$ Electronic partition function for *jth* orbital of species α

γ Adiabatic ratio of specific heats

$\Delta I_{j\alpha}$ Reduction in *jth* ionization potential of species α due to non-idealities

ε_0 Permeability of free space

η Efficiency

λ_d Debye length

Λ deBroglie wavelength

ζ	Damping coefficient
ρ	Density
Γ	Ablation rate
σ_{elec}	Electrical conductivity
σ_s	Stefan-Boltzmann constant

Chapter 1

A Brief History of Conventional and Electrothermal Launchers

1.1) History of Propulsion Weapons

Since the beginning of mankind, the fabrication and usage of tools for survival has been distinctive to humans and has set us apart from the rest of the animal kingdom. Ranged weapons were first introduced in the simple fashion of thrown sticks and stones during the Stone Age as a means of hunting and self-defense from predators. Lacking in both force and range, the ingenuity of man quickly began to develop new ideas to better long range technologies. Slings were brought forth very early and can be traced back to the Neolithic Era or even the Late Stone Age [2], giving man a large tactical advantage with a range as far as 400 m with a small stone [3]. Very shortly after the sling came the invention of the bow and arrow, dating back approximately 64,000 years ago [4]. The simple bow was quickly re-designed to improve its features with the addition of laminated layers to strengthen the bow material and increase force. Composite bows, seen in Figure 1, then improved upon this idea by using three separate types of materials in the laminated layers to increase the bows elasticity [5].

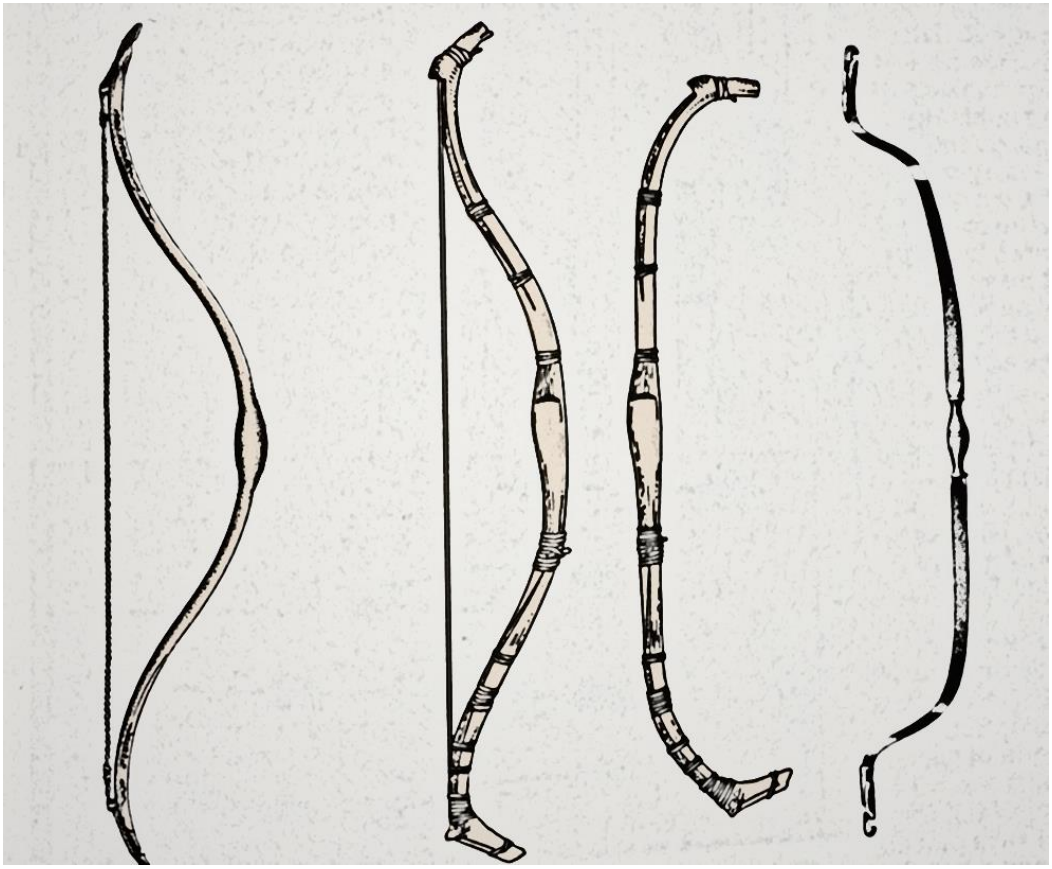

Figure 1-1 Forms of the Composite Bow

1.2) Chemical Propulsion Launchers

Leading into the invention of gunpowder was the earlier formed explosive known as black powder. Dating back to as early as the Sung Dynasty (A.D. 960) in China, black powder was very commonly used, possibly even for rocket based weapons. Very little is known about the very first explosion in a crude conventional weapon, other than it probably happened in North Africa. The first conventional weapon that can be traced back goes to the times of the Dark Ages and is credited to Arabic scientists.

The earliest form of cannons was introduced during the 13th century feudal period, 1240 to 1250, in Europe. Many vast socio-economic changes came quickly as dukes, barons, and other nobles sought to overthrow their tyrant kings. These new cannons proved to be successful in battle, not because of their destructive force, but rather the explosion, flames, and even the smoke itself brought terror to the knight and his horse, along with other enemy forces. The projectiles launched were stone balls, which hardly damaged the heavily armored knight and did nearly nothing to large castle walls. By the 14th century, cannons had been designed to be larger and much more powerful leaving knights vulnerable and castles defenseless [6].

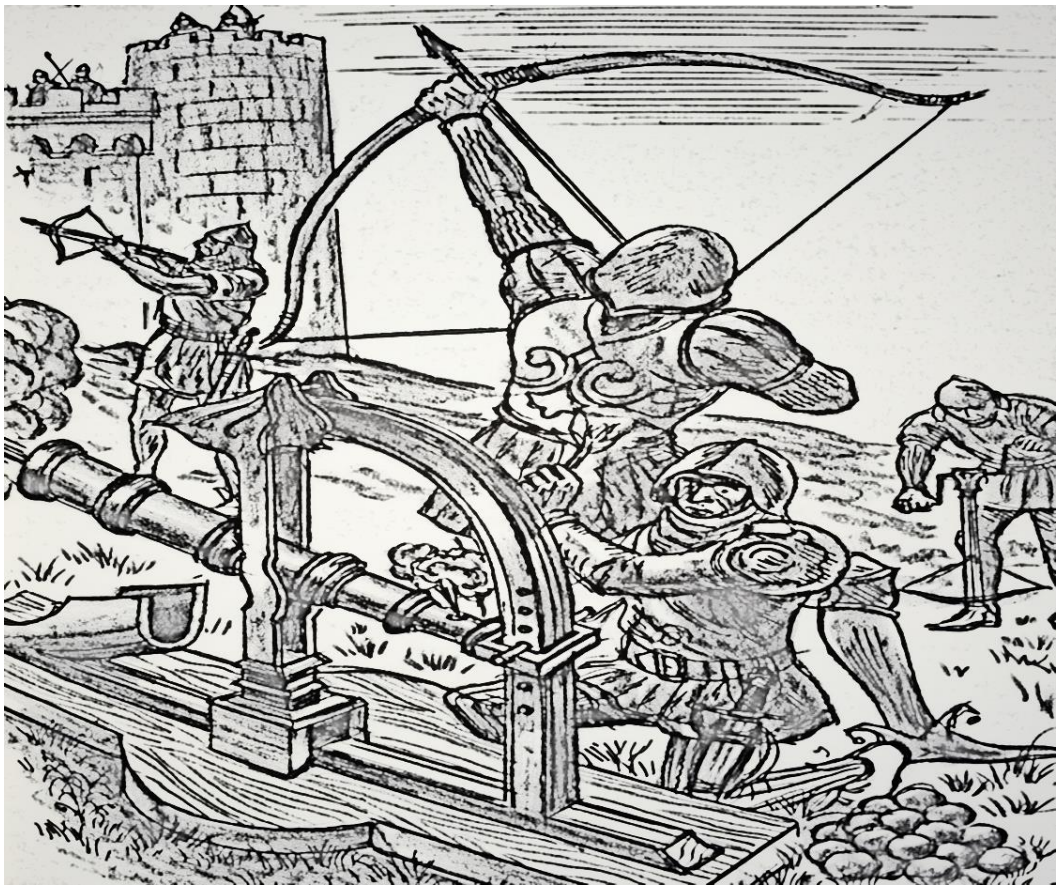

Figure 1-2 Medieval Conventional Launcher

Serpentine powder, a more refined and powerful version of black powder, was introduced around 1450. The serpentine powder was very finely ground, which allowed for a faster explosive reaction to occur, thus giving a more powerful projectile launch, but also was more dangerous to the user by its ability to form dust clouds which would explode at any spark. Some setbacks included that the powder needed to be firmly compressed in the cannon, but not so compressed that certain areas would not ignite. Also, the serpentine powder left high concentrations of unburned carbon in

the barrel, delaying the reloading process. After just half a dozen shots the cannon needed to be scraped and scrubbed out. Corned powder was a creation born of serpentine powder, yet far superior. The basic idea was to take serpentine powder and create a wet mixture, and then allow it to dry in order to create larger grain, thus allowing the combustion reaction to spread more quickly. The dried powder was pressed into the form of a small cake, which allowed for safe transportation. However, due to its overwhelming power, it was not used until the late 1600's when the materials of the cannons were strong enough to contain the explosive force. The projectiles were also changed so that they could withstand the blasts. Initially, stone balls were dipped in bronze, and later became fully cast iron as manufacturing technology developed [6].

Modern gunpowder cartridges with metallic casings came about around the 1850's. During this time, Walter Hunt filed a patent for a new bullet for a new repeating gun. His two patents became the basis upon which many designs are built today. The basic principle of his design was a cylindrical shell which houses the propellant and is sealed shut with the bullet acting as a plug itself. This allowed for reloading times to be significantly reduced by the availability of a ready to fire projectile. Hunt's other invention was the straight-drive firing pin, which in combination with his bullets allowed, for the first time, rifles to be considered rapid fire [6]. Needless to say the projectile itself has shrunk as well due to contributing

factors of accuracy improvements, materials used, and better propellants. All of these factors have given rise to what we now know today as the conventional launcher.

1.3) Electromagnetic Launchers

The first official studies of electricity are credited to an English physician named William Gilbert. He distinguished in 1600 the lodestone effect from static electricity developed by rubbing pieces of amber together [6]. Following in 1660, Otto von Guericke of Germany developed a machine that could produce electricity; the first electric generator. Very quickly, electricity became a popular phenomenon of interest to many scientists. This lead to the development of electromagnets by Joseph Henry in 1824 when he was the first to display the extended power of a magnet when wound with insulated wire and excited. Henry also designed the first magnetic engine; a reciprocating-bar motor powered with a battery, and developed many of the ideas behind the electric generator [8].

The term “battery” was first used by Benjamin Franklin in 1748 to describe an array of charged glass plates. Franklin worked with the Leyden Jar in many of his experiments and soon found that a flat piece of glass performed just as well as the jar, leading him to develop the flat capacitor. Soon afterwards Michael Faraday created practical capacitors which stored any unused electrons in the capacitor’s electric field during his experiments

[9]. Energy storage thereafter was the driving force for many applications to follow.

In 1844 the first electrical launcher was introduced. Siva, or “The Destroyer”, was featured by the British Navy in effort to replace the conventional weapons. The advertisements for the electromagnetic launcher read, “The balls are projected in a continuous stream at a rate of more than 2,000 per minute, each ball having force enough to kill at a greater distance than a mile with certain aim, and continue from year to year at a cost far less than gunpowder, although with more force.”[10] These were very strong claims, but not much was known about how it operated or functioned and the device did not live up to its potential, never to be seen again. The first serious attempt at developing an electromagnetic launcher comes from Birkeland of Norway. Patented in April, 1902 Birkeland details his model for an electromagnetic launcher, including the size and power he was hoping to achieve [11].

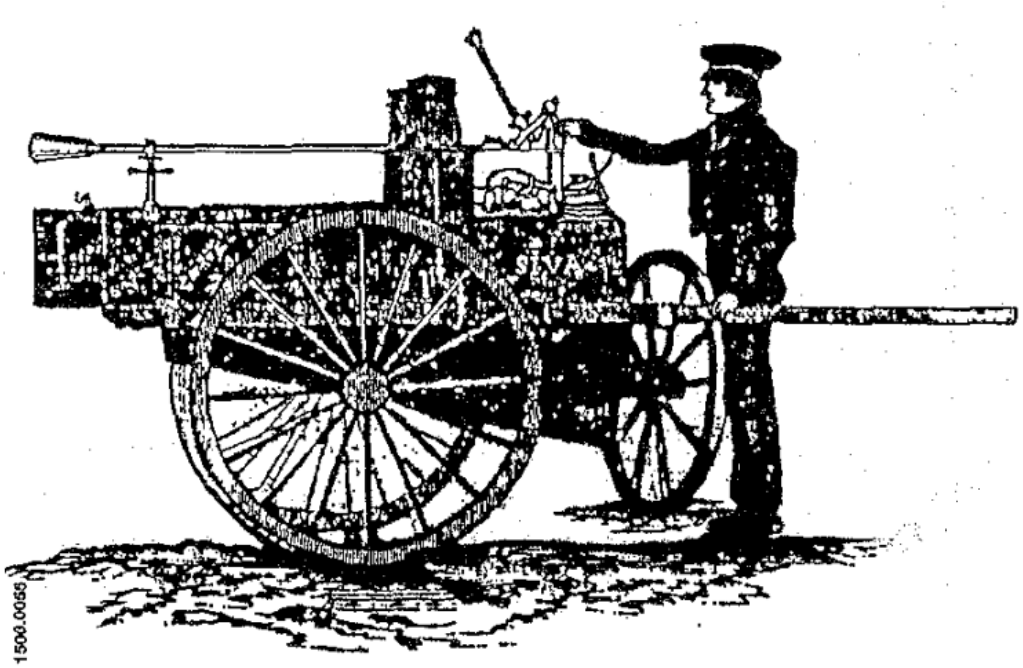

Figure 1-3 Siva

Fauchon-Villeplee began studying railguns in France during World War I. He demonstrated a small model of his railgun to the Director of Inventions at the Ministry of Armaments in 1918 by launching a spiked projectile into a wooden block. Having impressed the director, Fauchon was given the task of developing a 30-mm model and a 50-mm model. Fauchon's work solidified many ideas about the railgun, but he was cut short of his research when the project was abandoned at the end of World War I. His model demonstrated a railgun with a barrel length of two meters, a projectile 270 millimeters long, 70 millimeters wide, weighing 50 grams, and with a firing velocity of 200 meters per second. To launch the projectile with those specifications would require a 50 volt source with a peak current of

5,000 amps. Other concepts introduced by Fauchon include that of an iron-free system (or air-core system), a homopolar generator, and support frames to balance the reaction forces [10].

Professor Korol'kov of Russia was another who made many large contributions to electromagnetic launchers. Among his claims were system efficiencies, lifetime response, and detailed physics equations to better understand what was happening within the system. He concluded with a suggestion to change the energy storage to capacitors and batteries rather than fly-wheels, which to this day has been the main approach in building an electromagnetic launcher. He noted on the topic that "an electrical station… of special design of enormous capacity (which is) very heavy and complex", and still to this day proves to be one of the major issues [10].

In 1921 MacLaren's patent was a major contribution in the United States for electromagnetic launchers. His concepts of the coilgun barrel showed the projectile could be accelerated down the entire length of the barrel given a very large current for an extended period of time. This of course would require a power supply large enough to deliver such a current pulse, which was suggested that a very large flywheel be used to store the energy. However significant research wasn't done until 1945 during World War II when Dr. Hänsler and Dr. Muck of Germany were experimenting with power supplies. They experimented with capacitors, pulse transformers,

batteries, and pulse generators and reached the conclusion the homopolar pulse generator was the best way to store energy. Though their solution was capable of producing an output of 1.5 MW, it was not adequate or practical for military use as the power supply weighed over 150 tons [10].

1.4) Conventional Launcher Concepts

The first compressed air gun, dating back to near 1580, is a simple conventional launcher. To produce a propellant force air is compressed into a reservoir by means of a mechanical pump where it is stored as potential energy. When the seal of the reservoir is broken the system begins to move towards equilibrium by releasing the compressed air, with a high potential energy, into the barrel where the air is already at a near equilibrium state with no potential energy. The result of the two environments combining is generation of a kinetic energy which then is used to induce a force and moves the projectile. The force can be expressed as the total pressure P distributed over the normal surface area A.

$$F = P \cdot A \qquad \text{Equation 1}$$

To enhance the abilities of the compressed air gun, springs have been added to achieve higher exit velocities. Certain spring-piston launchers have been able to achieve speeds greater than that of the speed of sound.

To achieve such speeds a coiled steel spring, contained within the compression chamber, is compressed by a piston until a hook near the end of the chamber secures the spring in a compressed state. When the trigger mechanism is released the spring decompresses and pushes the piston forward. The result is the air behind the projectile is compressed and undergoes an adiabatic process where the air is heated to several hundreds of degrees and then cools as it expands. The rise in pressure generates a force, and propels the projectile forward [12].

Certainly a rifle launching a bullet from a gunpowder explosion is similar to the compressed air gun as air is the working fluid used to accelerate the bullet. The concept of air being at a higher energy here however is due to the explosion of the gunpowder, which heats the air and then causes expansion. Then energy, as before, is transferred from the higher state of the explosion into the barrel, and it pushes the bullet forward, as it moves towards a state of equilibrium. The explosion only last for hundreds of microseconds, and the force behind the bullet is still related to the pressure behind the cross sectional area of the bullet. With such a short explosion however, there is a limited amount of time for energy to be transferred as the bullet begins to travel down the chamber immediately and the system returns to equilibrium. The force behind the bullet would have a resulting acceleration profile resembling a short pulse, with a large peak,

and the resulting muzzle energy would be equal to one half the mass of the bullet, *m*, multiplied by the muzzle velocity, *v,* squared.

$$E = \frac{1}{2}mv^2 \qquad \text{Equation 2}$$

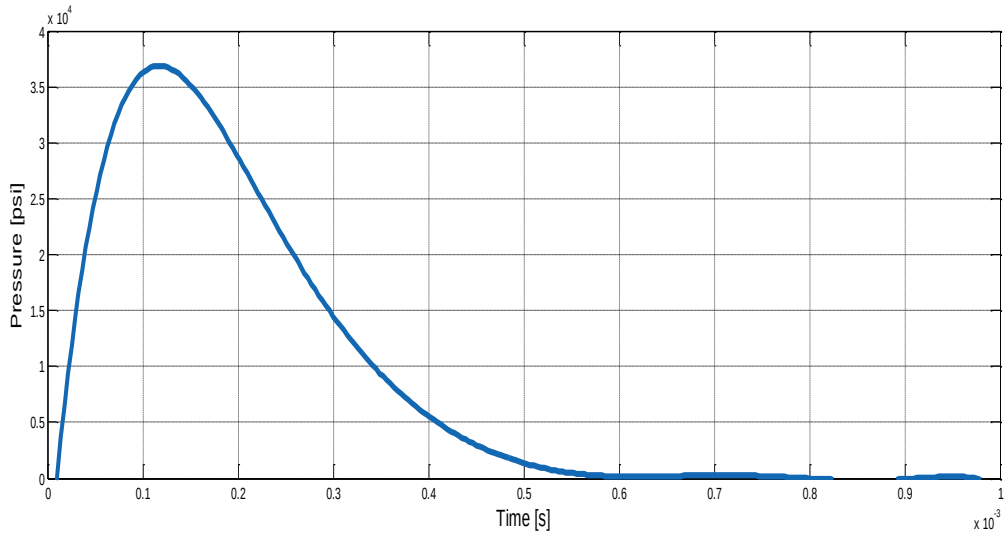

Figure 1-4 Pressure Profile of Gunpowder Explosion

Because the pressure pulse is limited to a single explosion, control is limited. Primarily the exit velocity is limited to the peak pressure, as the pressure acts as the driving force and is no longer able to keep accelerating the bullet down the barrel past the peak of the pressure pulse. This is because the bullet is already traveling near its terminal velocity by the time the pressure peak occurs, thus it is traveling just as fast as the air traveling behind it. When the bullet travels at the same speed of the air behind it there

is no longer a pressure differential meaning there is no more force being applied to the bullet.

1.4.1) Light Gas Guns

The (two stage) light gas gun works on the same basic principles as the spring-piston launcher. However rather than a spring driving the piston, a chemical reaction is the driving force behind the piston. A common propellant would be gunpowder. Also, the working fluid pushing the projectile is a lighter gas, such as helium or hydrogen. The reason for a light gas is because the pressure wave cannot travel faster than the speed of sound, so in order to increase the speed of sound a new medium is chosen. For helium, that value is 3 times greater than that of air, while hydrogen is 3.8 times greater. Temperature is also directly related to the speed of sound in that a higher temperature will yield a higher speed of sound. So while the air is being compressed, as mentioned before, it undergoes an adiabatic heating process and serves to increase maximum projectile speed. Another differentiation in the light gas guns is that they use a highly calibrated rupture disk to act as a valve to ensure maximum energy transfer. When the pressure build up is significant enough, the rupture disk will tear, then allowing the compressed high pressure, light gas to pass into the barrel [13].

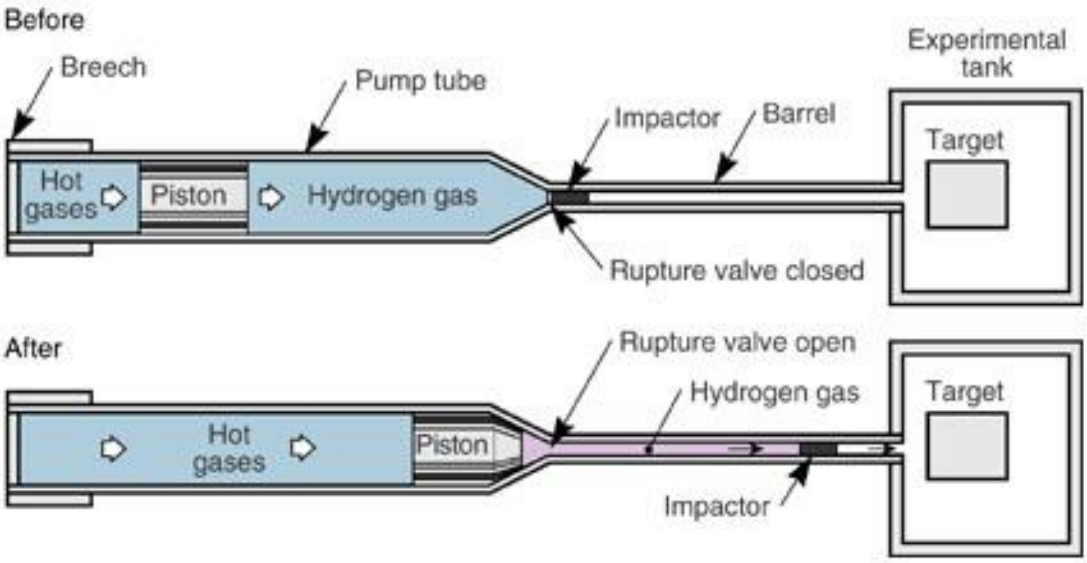

Figure 1-5 Light Gas Gun Diagram

Combustion light gas guns are similar to light gas guns in that a light gas is used as a medium to transfer energy from the increased pressure. However, the propellant used utilizes the high explosive force of low molecular-weight combustible gases. Gasses, such as a mixture of hydrogen and oxygen, are typical choices. The gasses, when ignited, will burn at higher temperatures with higher efficiencies than a solid propellant. For gaseous propellants the specific impulse, or force, with respect to the amount of propellant used per unit time, is also increased and higher exit velocities can be achieved. However, the drawback to such a design is a lack of uniform and predictable ignition, thus making accurate calculations for exit velocities near impossible. Another trouble with the combustion light

gas gun is that the projectiles must be hardened to remain intact from the very high acceleration it undergoes.

Figure 1-6 Ultron's Light Gas Gun

1.5) Electric Launcher Concepts

Beginning with the most common type of electromagnetic launcher is the railgun, where a current pulse is sent through two parallel conducting rails. The rails are shorted together by a metallic armature running between the two to allow continuous current flow. The material chosen to build the rails must be highly conductive, as very large current pass through, and should be able to withstand extreme forces from the violent acceleration of the projectile. From the current pulse, a magnetic force known as the Lorentz force is acting upon the armature, causing it to accelerate in the

normal direction. The Lorentz force is defined as the cross product between current density J and the magnetic field B.

$$F = J \times B \qquad \text{Equation 3}$$

An armature of plasma may also be used, where the two rails are connected by the arced plasma between them. Similar to the metallic armature, the plasma will be accelerated by the Lorentz force in the normal direction and push any mass in front of it. The first advantage of plasma armatures over solid armatures is the reduction of mass in the payload, which allows for greater acceleration due to less force required to move to payload, and also less friction acting against the payload. Such benefits will make hypervelocity travel more attainable. Another advantage is the reduction of bore damage, such as grooving, which significantly limits the lifespan of the rails [14].

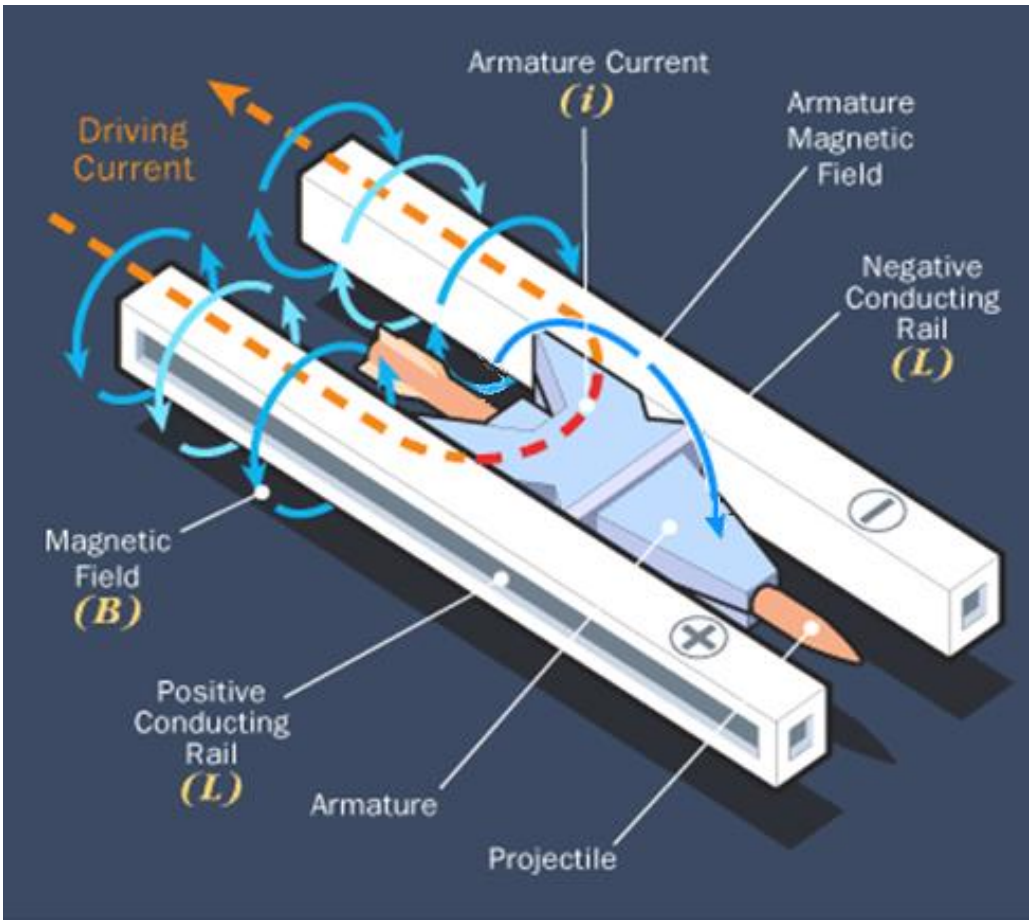

Figure 1-7 Example of Lorentz Force

It should be noted that railguns may act as a standalone system or as a pre-injector. As a pre-injector the railgun would act as the first stage in the system in which the projectile is initially at rest, and then pre-accelerated into the second stage to help mitigate damage to the system and increase system efficiency by ensuring more energy at the second stage is utilized. Applications for the railgun being investigated include space launch, or assisted space launch [15], military applications [16], and triggering of inertial confinement nuclear fusion [17]. An exceptional benefit for the

railgun is its ability to precisely control the acceleration of the projectile given the current pulse driving the system. With the capacity to store energy into separate capacitor banks, and then release each in a cascading movement, the ability to continuously apply a force to the projectile of a railgun, until it is no longer in contact with the conducting rails, is now achievable. A pulse forming network, which will be mentioned later in more detail, can produce a constant current, as seen in figure 8, throughout the entire duration of the firing process, or create a quick pulse similar with conventional launchers.

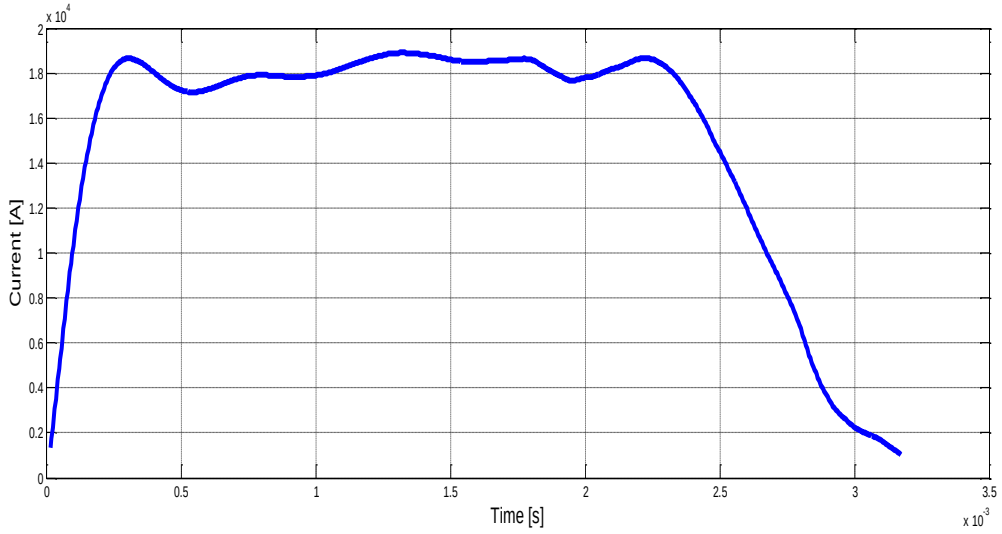

Figure 1-8 Simulated Railgun Discharge

Using a railgun as a standalone system can introduce challenges which can inhibit the lifespan of the railgun, rendering it useless after just a few shots. Often a pre-injector will be used to mitigate the damage to the railgun. A main concern with plasma railguns is re-striking of the plasma arc

between the rails after the projectile has already passed. Re-striking of the arc occurs when there is an excess of gas in the bore behind the projectile. The gas then acts as a medium for plasma to flow during voltage breakdown. Voltage breakdown occurs when the conditions within the bore approach the minimum of the Paschen curve for the given gas within the pre-injector [20]. The reason why re-striking has negative effect is that it draws current away from the main discharged arc. When the re-strike current tries to recombine with the main arc however the gas and ablated material are compressed between the two arcs which prevents the re-strike from recombining at all, thus wasting the current it drew away.

Bore ablation is another concern in railguns, particularly at or during launch. A high radiative heat flux develops from the discharge arc when the projectile is accelerated from rest. This heat flux will vaporize the outer material of the rail, and in turn the rails will become less conductive with each shot. Also the vaporized material will fill the bore with hot gas, and will become more probable to allow re-striking. By adding a pre-injector to the railgun, the projectile will already be moving thus allowing a path for the heat flux to travel and escape, and reduce the amount of damage done to the rails. Also the amount of additional material released into the bore from ablation is reduced which helps limit the impact of a re-strike.

1.5.1) Electrothermal Launchers

Another type of electrically propelled launcher is the electrothermal (ET) launcher, which relies on working heat to expand gasses in a chamber to accelerate a projectile. In order to establish the high temperature and pressure gas, the chamber is subjected to a capillary discharge. Initially, the chamber walls are lined with a lightweight polymer, such as polyethylene (PE). When exposed to the heat flux, generated by the exploding fuse and ionizing electrons flowing across the chamber, the discharge acts as the working fluid within the system by ablating and dissociating carbon and hydrogen atoms from the capillary wall. The ablated material will become partially ionized and generate a high temperature and high pressure propellant gas. The advantage of such a system is that safety factors are reduced as no explosives are used, and the capillary wall acting as the fuel source does not need to be replaced after each individual shot. There is a small increase in launch efficiency as well, due to the limited amount of propellant gas trailing the projectile, where less energy is dissipated as kinetic energy, or a drag force, in the propellant gas. Another key feature of the ET launcher is the ability to somewhat control the energy of the projectile, thus controlling its exit velocity, by adjusting shape and peak of the generated current pulse from the power supply [19]. A typical diagram of an electrothermal launcher can be seen in figure 9.

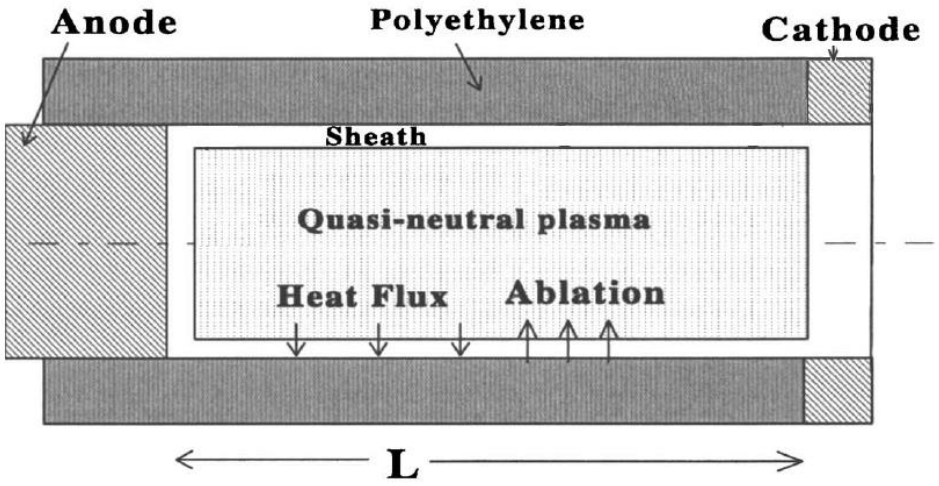

Figure 1-9 Electrothermal Launcher Chamber

1.5.2) Electrothermal-chemical (ETC) launchers

Electrothermal-chemical (ETC) launchers were developed from chemical launchers to achieve higher propellant gas sound speeds by improving the rate of expansion of the propellants. To do this, a plasma capillary, which consists of two electrodes with either a fuse or gas between them, is placed within or behind the propellant, as seen in figure 10. Then, a high voltage is applied to the electrodes until breakdown occurs between them and an arc is formed, thus igniting the propellant. The increase in performance of the propellant will reduce the effect of temperature on propellant expansion which allows for higher density propellants to be used, and pressure on the barrel will be reduced because of the propellant gas being distributed more uniformly within the system [18]. With the electrical

energy added into the working fluid, as opposed to solely using the propellant, exit velocities are estimated to be as much as 25% higher [17].

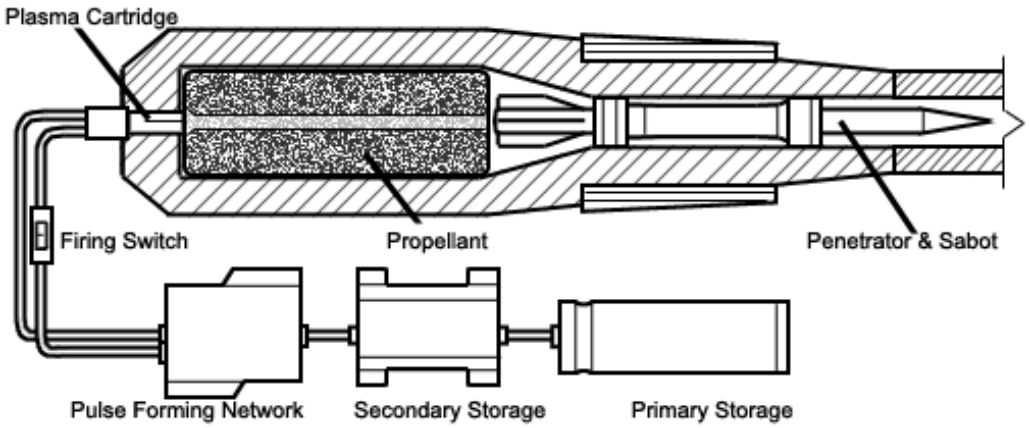

Figure 1-10 ETC Launcher Diagram

1.6) Comparison of Launchers

Conventional launchers and electric launchers each have their benefits and drawbacks. One main advantage for the conventional launcher is that it is relatively small compared to electric launchers when looking at the overall system. The propellant charge can be stored in small containers, whereas the electrical launcher requires large pulsed power supplies, in the form of capacitor banks or flywheels, to source the extremely high pulsed currents required. Another advantage of the conventional launcher is that there is less time between shots due to the propellant charge being readily

available. This can be compared to the electric launcher needing the pulsed power supply to be recharged before each shot.

The electric launcher, though, has many benefits of its own making it an advantageous solution. Safety is a large concern around such powerful devices, and reducing the risk of any accidents would make the device more appealing. With the pulsed power supply as an energy storage device, it only holds a charge right before firing. This means that the chances of a catastrophic event from an accidental discharge are reduced because the system energy is contained. With a conventional launcher, though, the propellant charge produces far more of a risk as it would only take a small spark to ignite the entire supply. Also, if the propellant has any contaminant in the mixture then performance will be severely crippled, possibly even making it impossible to fire a single round off. The result of a misfire due to contaminants would even make it necessary to decommission the launcher until the chamber is cleaned and well inspected to prevent further incident. This creates a special need to properly secure, seal, and transport the propellant charge at a greater expense.

Another compelling reason for the electric launcher is that a constant force can be applied to the projectile throughout the length of the barrel. The conventional launcher relies on a single large pulse to drive the projectile, which is inefficient for energy transfer, thus allowing the projectile to

succumb to losses, such as friction and drag, before it can exit the barrel. As explained previously the projectile in a railgun is driven by the Lorentz's force, which is a result of two currents moving in opposite directions. The current driving the projectile will continue to flow until the metal armature connecting the two rails of the barrel exits the system, creating an open circuit and stopping the current flow. This is a unique advantage in itself because it allows for more control over the projectile. By changing the magnitude of the current and the shape of the pulse there is a degree of control of the Lorentz force. Now, the ability to control the exit velocity and change it to meet the needs of the application in real time situations is possible with a pulse-forming network, which will be discussed later in detail.

1.7) Project Goals

The goal of this project is to produce a computational model, which predicts the exit velocity for an ET, or ETC launcher due to the mass of polyethylene ablated during a capillary discharge. From henceforth, the ET launcher of discussion shall be referred to as the pre-injector for a railgun. By adding a pre-injector stage onto a railgun it is possible to increase the magnitude of the acceleration profile, and reduce damage to the start-up section of the conductive railing. This is because in a standalone system for a railgun there is much energy wasted just trying to move the projectile from

rest. Also as mentioned before, the use of a pre-injector reduces the damage done to the rails by reducing the heat flux exposed to the rails, which can vaporize the conductors. Another benefit of the pre-injector is that it helps eliminate re-striking the arc between the rails as well. As the cold gas can increase the possibility of a re-strike, and hinder performance, the pre-injector has the ability to limit the amount of hot plasma being injected into the launcher behind the projectile. Applications for a pre-injector include hypervelocity launches in excess of 7 km/s for direct space launch [21], as well as military applications. To be able to better understand the behavior of a pre-injector the model will take into account all of the previously mentioned topics to best be able to predict the performance. Modeling a capillary discharge is no easy task, and many steps will be taken to further explain the derivations used in this model.

Chapter 2

Electrothermal Launcher Concepts

The setup for an electrothermal launcher consists of multiple parts. The pulse forming network, and pre-injector are of interest, as well as their interaction in ablating the wall material during discharge.

2.1) Capillary Discharge

In any electrically driven launcher, there is a need for an electrical power generation system which supplies the high current pulse to the capillary chamber, i.e. the launcher. In the case of railguns, electrothermal (ET) launchers, and electrothermal-chemical (ETC) launchers, a pulsed forming network (PFN) made up of lumped capacitors and inductors is typically used. The output shape and amplitude of the PFN's current pulse can vary considerably from application to application. In some cases a steady flat output with a steady peak is needed while in others a pulse with a high peak to average ratio is used. One nice feature of electrically driven launchers is that the output amplitude is typically easily varied by simply adjusting the initial charge voltage of the power supply. The next sections will discuss the PFN used here and the capillary itself. It should be noted here that the PFN and capillary were designed and built by researchers at Texas Research Institute (TRI) and the University of Texas at Austin (UT) both of which are in Austin, Texas. They were responsible for all

experiments and the collection of all data. The objective of the work in this thesis is accurately modelling the system and results they obtained.

2.2) Pulse Forming Networks

The PFN used here, seen in Figure 12, is capacitive based and utilizes only stray inductance to shape the high peak to average pulse delivered to the launcher. Capacitive storage is used because of the need for high peak power which normal grid tied power supplies cannot provide. The energy is sourced by a 20 kV, 300 mA grid tied power supply and stored in a capacitor bank over a period of tens of seconds. Six 206 µF capacitors are connected in parallel, as seen in figure 11, to form essentially one large capacitor from the viewpoint of the output. The equation for adding parallel capacitors is seen below, where n is the n^{th} number of capacitor.

$$C_{total} = \sum_n C_n = C_1 + C_2 + C_3 + \ldots + C_n \qquad \text{Equation 4}$$

In this case the total capacitance will be 1,236 µF. The stored energy in Joules, E, is calculated according to equation 2 where C is total capacitance of the capacitor bank in Farads, and V is the initial charge voltage of the capacitors.

$$E = \frac{1}{2} C V^2 \qquad \text{Equation 5}$$

The result of paralleling the capacitors is and RLC network which is heavily underdamped without the addition of an additional resistance. As

the capacitors used cannot be rung negative, 300 mΩ of resistance is added in the form of a high energy ceramic disk resistor on the output of each capacitor. This along with the stray inductance of the system critically damps the system so that the resulting output pulse is a single peak with a RL decay down to zero amps, over roughly hundreds of microseconds. Because of the losses in the system, including those internal to the capacitors, the buss work, and the added resistors, the energy delivered to the chamber is much less than that stored making this a low efficiency system. The energy actually delivered to the capillary is calculated by integrating the power dissipated in the chamber with respect to time.

$$E_{capillary} = \int_0^t V_{capillary} I_{capillary} dt \qquad \text{Equation 6}$$

At full charge, each capacitor can store roughly 50 kJ though they are never charged near this value in the application discussed here. In fact the power supply design here is terribly inefficient for this application. A capillary discharge would be much more efficient with lower voltage capacitors however, the ones used were the ones available at the time due to limited budget constraints. Despite that it is important to conceptualize how much actual energy is stored. To put it into perspective, it would take 100 kilojoules of energy to push a car with a force of 10,000 Newton, or 2250 pounds force, a distance of 10 meters. Keep in mind that the high electrical

energy being stored here is being transferred into object weighing only a few grams.

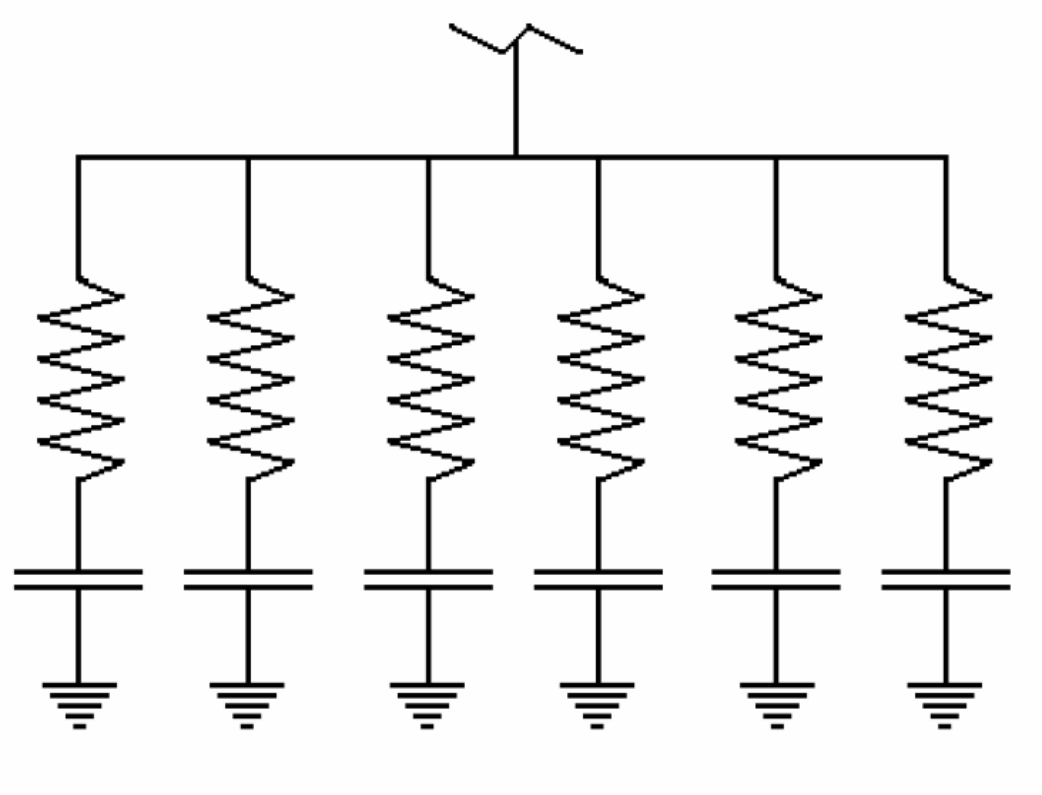

Figure 2-1 RC circuit for Power Supply

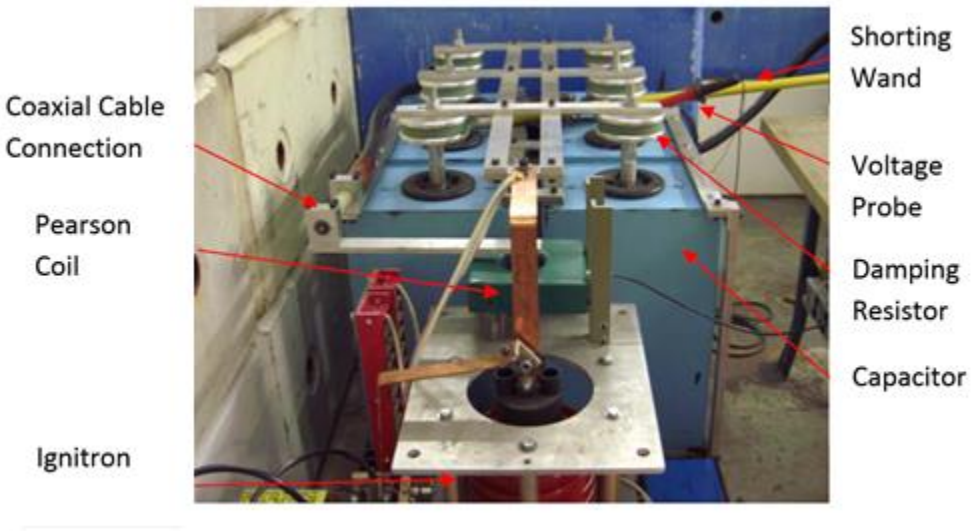

Figure 2-2 Pulse Forming Network Setup

Once the energy is stored, it must be quickly switched to the load. This is accomplished by placing an ignitron, which is essentially a large mercury switch, in series between the capacitor bank and the load. Housed within a heavy steel containment and placed within the pool of mercury is a stock of metal, which acts as the switch's cathode. Above the pool of mercury is another large refractory metal cylinder which makes up the anode. An ignitor, which is a metal electrode made of a refractory semiconductor such as silicon carbide, is placed just above the pool of mercury and it is briefly pulsed with a high voltage, high current source and its potential is applied with respect to the pool of mercury. This results in a plasma breakdown between the ignitor and the pool of mercury which causes the mercury to vaporize and form an electrically conducting bridge between the anode to cathode. The source's energy is discharged to the

load initially through this mercury vapor but this quickly transitions into a bulk plasma through which the current flows. One downside to an ignitron switch is that once conduction begins, it cannot be halted until a current zero occurs. A conceptual drawing of an ignitron is shown in Figure 13.

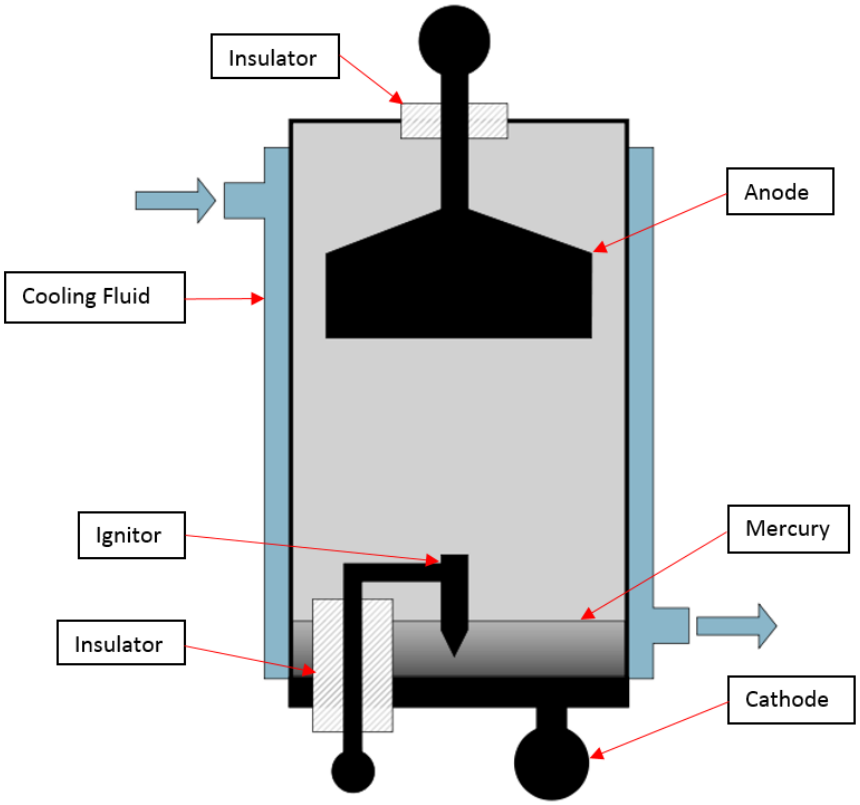

Figure 2-3 Ignitron Schematic

Initially all of the experiments were performed without a pulse shaping inductor between the capacitive source and load. Later in the testing phase, a 16 μH inductor was connected at the source's output in order to increase the pulse's rise and fall time. This essentially widens the acceleration profile

of the projectile. The series resistance with each capacitor is halved when the inductor is added to maintain the current amplitude and dampening. The output voltage for a RLC can be described as follows, where *i* is the current, *q* is the charge in the capacitor, *L* is the inductance, *R* is resistance, *C* capacitance, and *V* is the output voltage.

$$V = L\frac{di}{dt} + Ri + \frac{q}{C} \qquad \text{Equation 7}$$

With the inductor in series the dampening of the circuit changes. The resonant frequency of the system, ζ, will now vary with the circuit parameters and is given below for a series RLC circuit. Figure 14 displays different examples of the dampening coefficient.

$$\zeta = \sqrt{\frac{1}{RC} - \left(\frac{R}{2L}\right)^2} \qquad \text{Equation 8}$$

In both cases, the RC and RLC setups respectively, the circuit is over damped as a result of the added resistance.

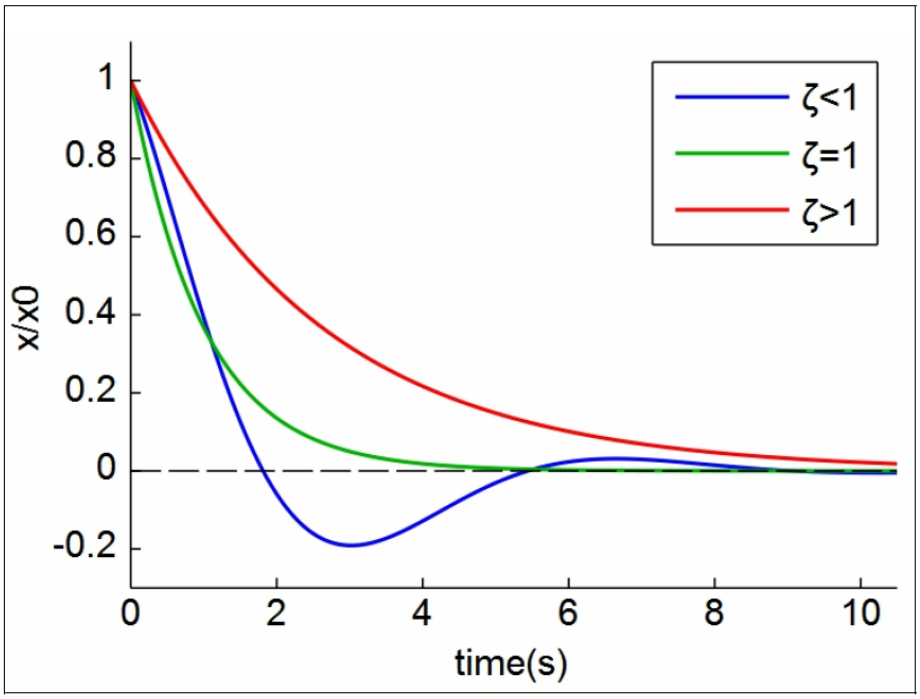

Figure 2-4 System Dampening

Remembering that current control is one of the main benefits for electrically driven launchers, there are multiple methods that can be used to adjust the output current of the power supply. The series resistance and inductance can be varied easily to adjust the current magnitude and pulse shape, i.e. the acceleration profile. The driving force is the energy stored within the prime power supply. That energy is easily adjusted by altering the capacitor's initial charge voltage enabling the velocity of the projectile to be adjusted by methods other than altering the barrel launch angle. Also multiple power supplies may be added to cascade current to extend the length of the pulse, as seen in figure 15.

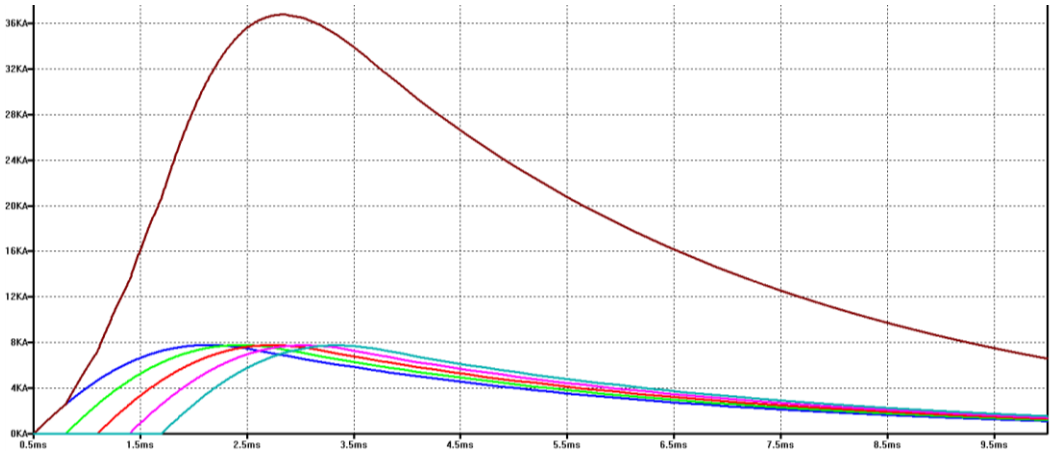

Figure 2-5 Cascading Power Supplies

2.3) Pre-Injector

The pre-injector is made up of a few components, seen in figure 16 below. The first is a thick walled hardened AISI 4140 steel chamber, inside of which is a thin walled polyethylene liner, which serves as the ablated material source for the capillary discharge. It is here that the current is fed in, the capillary's plasma is formed, and the pressure which accelerates the projectile is developed. Initially the high pulsed current flows through a thin, ~25 μm, aluminum wire fuse which connects the cathode of the chamber to the anode. The pulse application causes the wire to explode within the first few μs and a plasma arc to be sustained between the cathode and anode for the remainder of the current pulse. The arc ablates a controlled amount of polyethylene from the liner and rapidly heats it to a high temperature. The fuse initially has a resistance between 10 to 15 Ω. As discussed in the background section, capillary discharges work off of the principal of thermal

ablation which is essentially the vaporization of a material. The temperature of the plasma developed inside the polyethylene liner can reach temperatures in the range of 20,000 K. This is hot enough to transition the solid polyethylene into gaseous form. Initially the chamber starts out at atmospheric pressure however, the conversion of polyethylene to gas quickly fills the chamber, which is sealed at one end by an electrode and at the other end by the projectile, with a high volume of gas. This quick formation of gas results in the buildup of an intense internal pressure within the capillary chamber that eventually causes the projectile to accelerate through the barrel. Both electrodes are made of a 70/30 copper/tungsten alloy to allow for high electrical conductivity but also prevent melting.

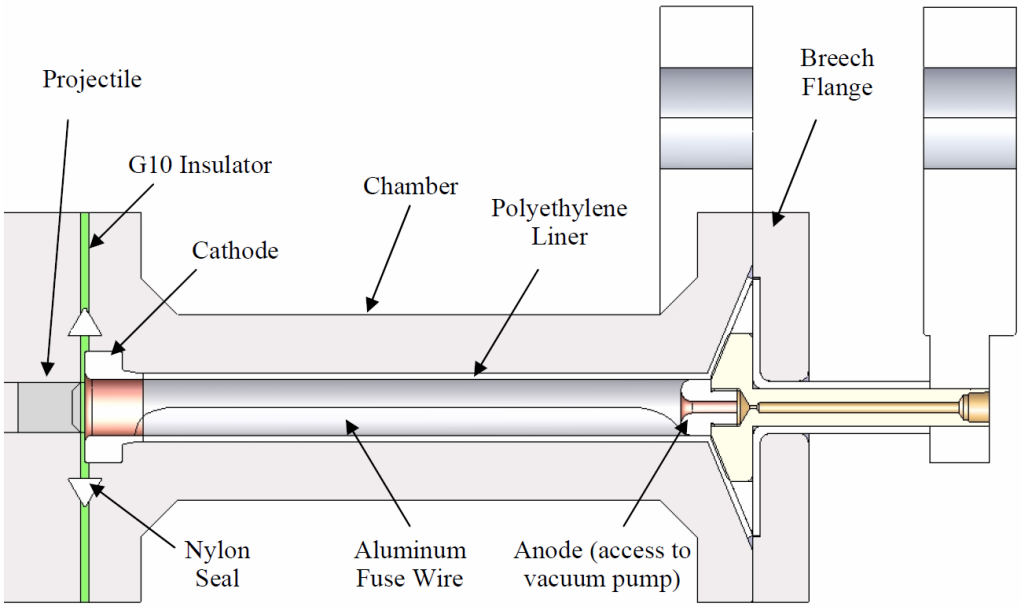

Figure 2-6 Pre-injector Schematic

As already discussed, current initially flows through a coaxial cable from the power supply and into the anode of the chamber. The fuse quickly blows and initially there is not always enough energy behind the plasma to transition it into a bulk plasma breakdown. This results in a short dropout in the current pulse referred to as a current pause, seen in figure 17. This lasts for around 1 μs, as seen in the sample waveform of Figure 17, after which the air has become more polluted to the point where the plasma has enough energy to finally breakdown the bulk dielectric [22]. The plasma imparts a uniform high radiative radial heat flux on the liner which ablates the polyethylene liner and releases a mixture of carbon and hydrogen gas, which is both neutral and ionized, into the chamber. From an electrical perspective, the current returns back to the power supply ground through the walls of the steel chamber. The process of ablation will be discussed in more detail later.

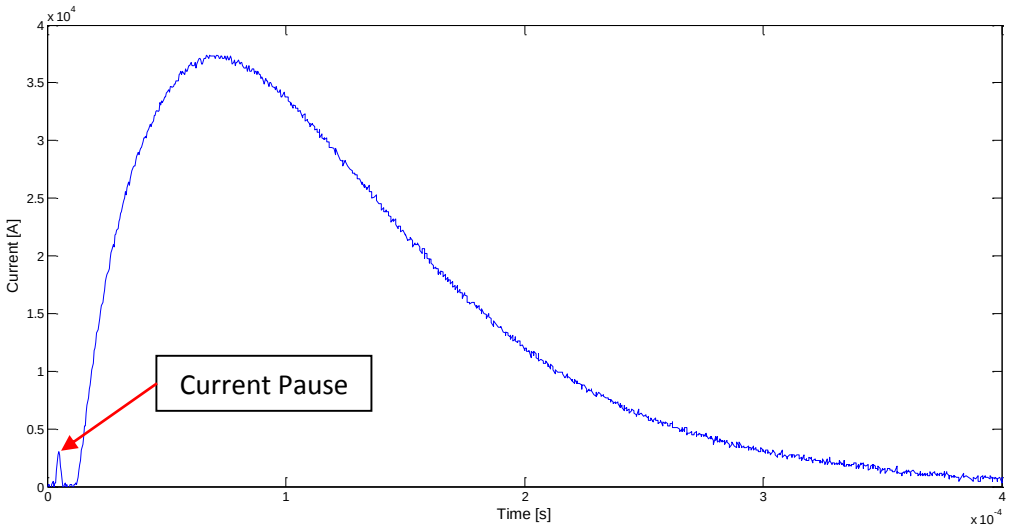

Figure 2-7 Current Pause

In many ET or ETC applications, the chamber and barrel are initially evacuated before the launch. The reason for this is that a plasma will be stronger, more conductive, in a vacuum environment. The removal of heavy ions from the environment enables ions to travel faster and collide with higher kinetic energy thus increasing the ionization of the plasma. The result is a hotter plasma which imparts more heat flux, ablates more mass, and accelerates the projectile to faster velocities [23]. While the evacuated chamber has all these positive influences, it is more difficult to implement and requires time between shots for a vacuum to be reestablished. Because rep-rate operation is of interest here, the chamber has not been evacuated but is instead operated at atmospheric pressure. The next reason being that molecular mass of the plasma will be reduced because it will consist mainly of carbon and hydrogen rather than air. Figure 18 displays the

different ion densities of mainly carbon, and hydrogen. Figure 19 shows a scaled version of the hydrogen ion density.

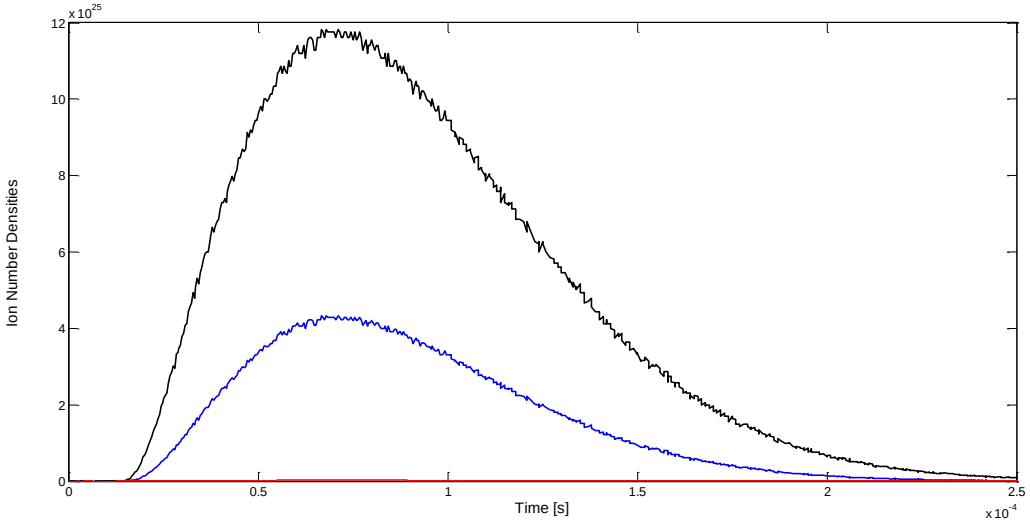

Figure 2-8 Ionization Proportions

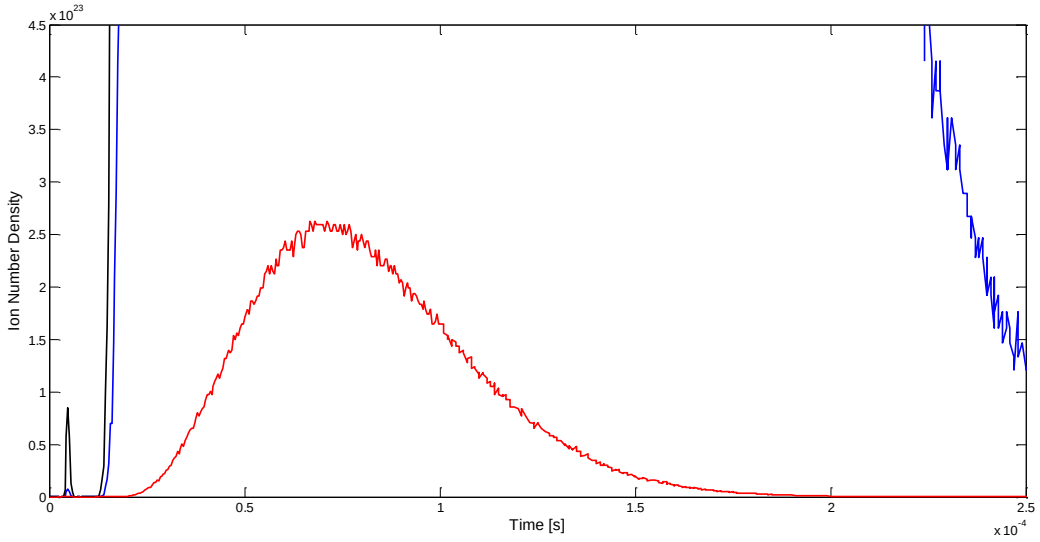

Figure 2-9 Ionization of Hydrogen

The pre-injector barrel consists of two sections; the initial section where acceleration takes place, and a free flight section. The acceleration section rests next to the chamber and is separated by a thin G10 insulator to prevent the arc from attaching to it. There sits a nylon seal between the chamber and barrel to prevent hot gas from escaping through the joints. The projectile rests immediately at the start of this acceleration section. The free flight region is then exactly as it sounds, just a long region through which the projectile accelerates. This free flight regions has thinner walls as the pressures in this region are not as severe.

2.4) Ablation

The formal definition of ablation as given by NASA is "*The removal of surface material from a body by vaporization, melting, chipping, or other*

erosive process" [24]. In this study the focus is on the first two, i.e. vaporization and melting. As mentioned before, a high radiative heat flux is formed as a byproduct of the ionization process. The heat flux is responsible for vaporizing and melting the outer layer of polyethylene, thus ablation occurs.

Since low density polyethylene has the chemical composition C_2H_4, the result of ablating polyethylene is a release of carbon and hydrogen into the chamber. The released particles have two functions. The first function is that the particles are ionized and contribute to the plasma formation. The distribution of dissociated and ionized particles can be approximated by the Saha equations which are based upon the energy in the system. Certain elements have ionization potentials given which can then be used with other system parameters to determine what percentage of the elements will contribute an electron, and for carbon some may be doubly or triply ionized. Governing equations concerning the Saha equations will be explained in a later section.

Dr. Michael Keidar and Dr. Iain Boyd have done extensive research to better understand the study of ablation in a capillary discharge for electro-thermal launchers, specifically concerning the Knudsen layer. In magneto-hydrodynamics the Knudsen layer is given to be the non-equilibrium, or kinetic layer, formed near the ablated surface which determines the ablation

rate. In their studies they have developed an analytical model of the Knudsen layer which takes into account the temperature gradient of the plasma, which they refer to as the bulk gas. Using the temperature gradient of the plasma a velocity distribution function is formed at the outer boundary of the Knudsen layer, which preserves the laws of conservation of mass, momentum, and energy [25].

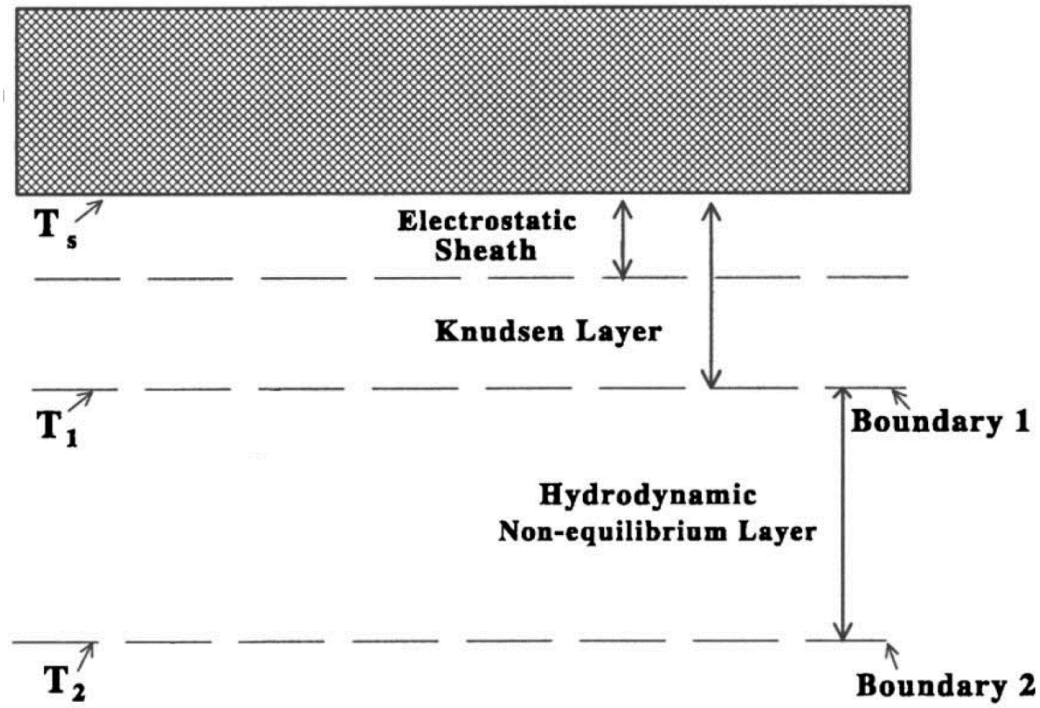

Figure 2-10 Knudsen Layers

Solving the continuity, momentum, and energy equations, referenced in equations 9, 10, and 11, for a 1-D axisymmetric capillary of length *L*, and radius *R* will yield a solution for ablation rate. Given that *x* is the spatial variable ranging from 0 to *L* the model assumes that all flow parameters will

be uniform in the radial direction for each layer of the model. The following equations are given for the Knudsen layer.

$$A\left(\frac{\partial p}{\partial t}+\frac{\partial pU}{\partial x}\right)=2\pi R\Gamma \qquad \text{Equation 9}$$

$$p\left(\frac{\partial U}{\partial t}+U\frac{\partial U}{\partial x}\right)=-\frac{\partial P}{\partial x} \qquad \text{Equation 10}$$

$$p\left(\frac{\partial \varepsilon}{\partial t}+U\frac{\partial \varepsilon}{\partial x}\right)=-P\frac{\partial U}{\partial x}+Q_j+Q_r-Q_F \qquad \text{Equation 11}$$

Fluid density, velocity, and pressure are given by *p, U,* and *P* respectively. The capillary cross sectional area is given by *A,* and the ablation rate is given as Γ. For the third equation concerning energy, ε is given in the equation below, where T is the plasma temperature, and m is the mass of the average fluid particle.

$$\varepsilon=\left(\frac{3}{2}\right)\left(\frac{T}{m}\right)+\left(\frac{U^2}{2}\right) \qquad \text{Equation 12}$$

The influx of energy to the plasma from Joule heating is $Q_j={}^{j^2}/_{\sigma}$, where *j* is the current density and σ is the electrical conductivity. Q_r and Q_F are energy losses from plasma radiation and convection to the wall. The pressure in the hydrodynamic layer is assumed to be constant during the process due to the high pressure in a relatively small volume, thus ${}^{\partial P}/_{\partial U}=0$. Also plasma temperature is assumed to be uniform throughout the capillary which makes ${}^{\partial T}/_{\partial x}=0$ [26].

To understand the heat conduction, radiation, and convection heat fluxes are transferred from the plasma to the capillary wall. The temperature inside the polyethylene is calculated with the following heat transfer equation, where *a* is the thermal diffusivity.

$$\frac{\partial T}{\partial t} = a\frac{\partial^2 T}{\partial r^2} \qquad \text{Equation 13}$$

This assumption is made in the one-dimensional radial direction and is made because the heat layer thickness near the surface is smaller than the curvature of the polyethylene cylinder, and is also less than the characteristic length of the plasma parameter, which varies in the axial direction. The next step is to determine the plasma composition, which is calculated using variables from the plasma density and electron temperature. Assuming that the polyatomic molecules fully dissociate, with an electron temperature between 1 and 2 eV, and a plasma density between 10^{24} to 10^{26} m^{-3}, only an ideal gas containing carbon and hydrogen is considered. Under the listed conditions it is expected the plasma will be in a local thermal equilibrium, or that the composition of plasma is determined by its local state and will be determined by the Saha equations. As the distribution of atoms, and electrons obey the Saha equations, the Saha equations should still be supplemented by the conservation of nuclei and quasi-neutrality [27].

Though sufficient for calculating the plasma composition, the Saha equations are only accurate in the case of an ideal plasma, but under high density conditions the plasma may become non-ideal. For the case of non-ideality, corrections to the ionization energies, partition functions, and plasma pressure are considered. To first determine the degree of non-ideality the following equation 14 is given where *e* is the charge of an electron, n_i is the number density of ionized particles or heavy particle density, n_e is the number density of free flowing electrons, ε_0 is permittivity of free space, and T_p is the plasma temperature.

$$\zeta = \frac{e^2(n_i+n_e)^{1/3}}{4\pi\varepsilon_0 T_p} \qquad \text{Equation 14}$$

If ζ is less than 0.1 then the plasma is considered to be an ideal plasma, but for values greater than 0.1 up to 1 the plasma is said the be weakly non-ideal. Therefore the corrected forms for ionization energy and plasma pressure are then given as follows, where *z* is the ion charge state, and R_D is the Debye radius.

$$\Delta I_i^z = \frac{(z+1)e^2}{4\pi\varepsilon_0 R_D} \qquad \text{Equation 15}$$

$$\Delta P = \frac{1}{6}\cdot\frac{e^2}{4\pi\varepsilon_0 R_D} \qquad \text{Equation 16}$$

The effective ionization energy for a high density plasma then can be expressed as $I_i^z = I_{ideal}^z - \Delta I_i^z$ and the plasma pressure is $P = P_{ideal} - \Delta P$.

Usually plasma composition is only affected and considered to be non-ideal if the heavy particle density is larger than 10^{26} m^{-3}, and plasma temperature is approximately 1 eV [27].

Solving the equations of the hydrodynamic layer of an ideal plasma will yield the following equation for the ablation rate.

$$\Gamma = mn_1\sqrt{\frac{n_2kT_2 - n_1kT_1}{mn_1(1-{n_1}/{n_2})}} \qquad \text{Equation 17}$$

In equation 17, for the ablation rate, *k* is Boltzmann's constant, *n* is the fluid number density, and *m* and *T* are as mentioned previously. Subscripts 1 represent values at the Knudsen layer to hydrodynamic layer and subscript 2 represents the hydrodynamic layer to the quasi-neutral plasma layer boundaries [28]. Not to be confused with the rate of ablation, the ablation rate as given above is also called the deposition rate and has units of kilograms per meter squared second, ${kg}/{m^2s}$. To take into account the entire system the ablation rate is divided by the length of the capillary for the rate of ablation, or total ablation.

In addition to the two-layer kinetic model, other studies conducted by Rui Li, Xingwen Li, Shenli Jia, and Anthony Murphy, two additional empirical numerical models were tested for ablation rates. The first is based upon Langmuir's law, "model-L", and is used mainly for switch apparatus arc

simulation. The second is based upon the assumption of ablation enthalpy, “model-E”.

In model-L it was assumed that half the particles will move into plasma and the remaining particles return into the wall of the layer adjacent to the wall’s surface. This means that only half of the plasma mass density will enter the bulk plasma, and the remaining particles will be distributed throughout the Knudsen layer and surface layer. Also the average velocity of the particles in this layer will have a component velocity equal to one half that of the velocity in any direction. Given these assumptions the ablation rate has the following form, where m is the mass of an electron, T_0 is surface temperature, and k is Boltzmann’s constant.

$$\Gamma = P_V \sqrt{\frac{m}{2\pi k T_0}} \qquad \text{Equation 18}$$

For polyethylene, P_V is a pressure state of equation for the plasma pressure. Because the system of equations is closed, if the equilibrium density at the ablating wall can be specified, the equation for P_V has the following form (exclusively for polyethylene) where A is 5565.22, and B is 453. However it should be noted that model-L makes the assumption that molecules are ablated in a vacuum rather than a dense plasma, and no particle back flux is taken into account, thus the ablation rate is normally overestimated. [29].

$$P_V = 10^5 exp\left[A \cdot \left(\frac{1}{B} - \frac{1}{T_0}\right)\right]$$ Equation 19

In consideration of electro-thermal chemical launchers, and plasma generators model-E was developed. This model assumes that ablation is caused primarily by radiated energy from the generated plasma. Yet only a fraction of the radiation energy is the cause for ablation in the surface layer, while the majority of the energy is reabsorbed into the bulk plasma and heats the capillary walls. The fraction of radiation energy used for ablation combined with a gray factor becomes the transparency factor, *f*. Assuming a gray-body radiation the ablation rate has the following form where σ_{sb} is the Stefan-Boltzmann constant, T_2 is the plasma temperature, and h_a is the ablation enthalpy. Model-E has been shown to agree well with experimental data due to the ablation enthalpy found to be near constant in many experiments, but there is an unrealistic time dependence in this model.

$$\Gamma = \frac{f\sigma_{sb}T_2^4}{h_a}$$ Equation 20

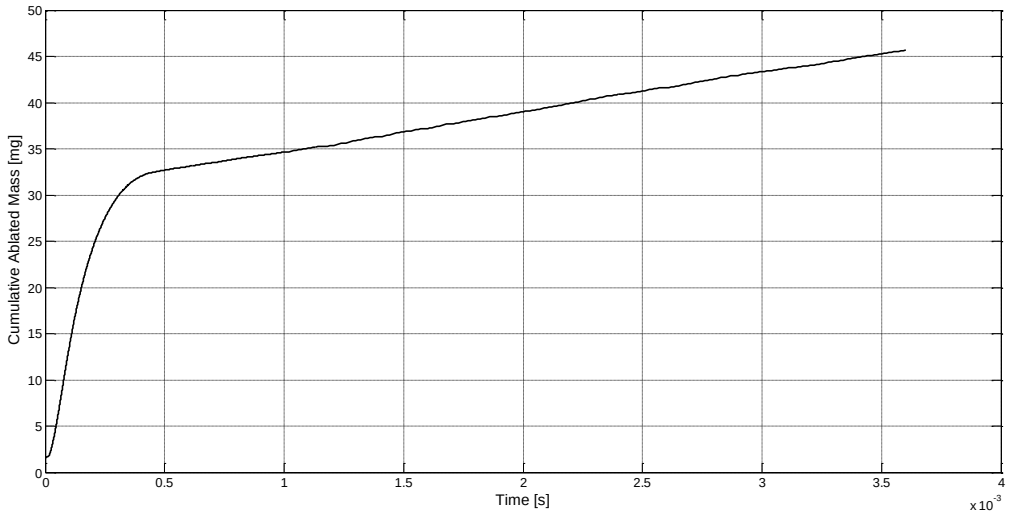

Figure 2-11 Cumulative Ablated Mass.

In the different models it should be noted that model-E only depends on the plasma temperature while model-L depends on the surface temperature. For the two layer kinetic model, model-K which was mentioned first, plasma temperature, surface temperature, and plasma density are all needed to solve for the ablation rate [30]. A cumulative rate of ablation simulated with model-K is shown in figure 21.

The ablated molecules now will act as the working fluid, or propellant gas, in the system to drive the projectile down bore as pressure increases. Also as the plasma heats the chamber, the polyethylene ablates carbon and hydrogen into the system, where both molecules are potentially ionized and contribute even further to the flow of plasma. The pressure being generated comes from molecules being released into the capillary chamber from the

heat flux of the plasma, and form an expanding gas. The rapidly expanding gas is what generates a pressure within the chamber, and is forced to exit out of the only opening, the breech of the pre-injector, accelerating the projectile down bore, as it is the only path for the propellant gas to travel.

Chapter 3

Plasma Characteristics

The different characteristics of plasma are determined by the current pulse, injected by the PFN. Through means of many equations, and iterative methods, it is possible to calculate certain values of plasma over a timed discharge.

3.1) Previous Research Models

The model developed for the research as described in this thesis was founded upon the technical report BRL-TR-3355, and every equation and description in this section is credited to the BRL report. John Powell and Alexander Zielinski were sponsored by the U.S. Army Ballistic Research Laboratory to develop a one dimensional model which would calculate the properties of plasma arcs in ablating, cylindrical capillaries. The objective was to provide understanding of plasmas which would then be coupled to models of both working fluids and the power supply of an electrothermal launcher. Primarily Powell and Zielinski were interested in extending the calculations for the time-dependent regime as traditional steady-state models have proven to be inaccurate in consideration of non-ideal plasmas as described earlier.

3.2) BRL Model and Assumptions

The basic model assumed in the calculations is shown schematically in figure 22.

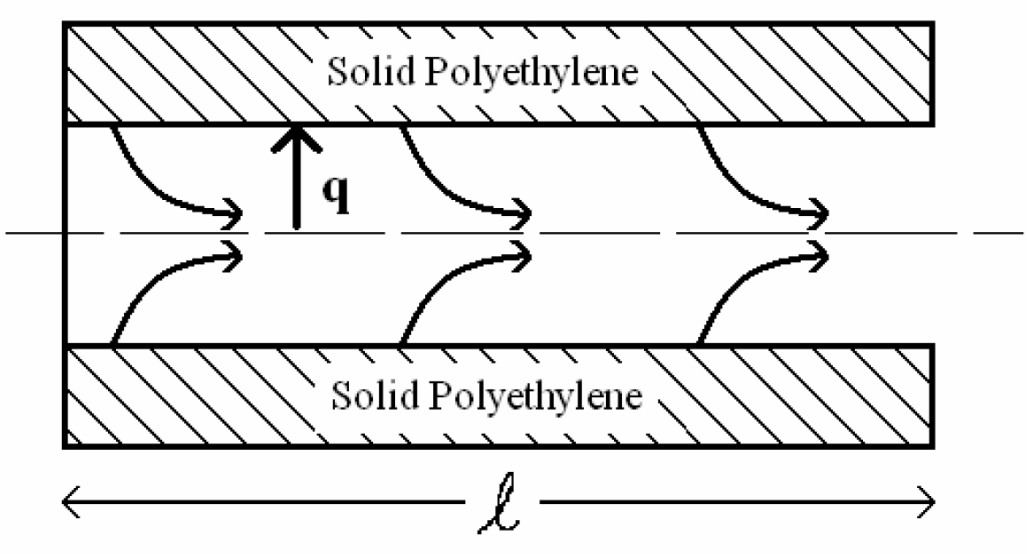

Figure 3-1 1-D Capillary Model

When a potential is applied to the anode, located at $z = 0$, and the cathode, at $z = l$, a current is produced, and is conducted through the plasma arc in the interior of the cylinder. The current will then rapidly heat the plasma via ohmic heating up to tens of thousands of degrees Kelvin. The resulting radiation heat flux of the plasma will then ablate material from the capillary wall. The ablated material will then begin to replace the plasma within the cylinder, and flow outward of the tube at $z = l$.

As mentioned before, the time-dependent model takes into consideration the non-ideality of plasmas. The non-ideal characteristics are important and should be considered when the plasma density is sufficiently high because of Coulomb interactions which cannot be neglected, just as the potential energy is non-negligible to the thermal energy. The result of a non-ideal plasma are as follows: Primarily plasma conductivity is reduced at fixed temperatures and pressures. The reduction is a result of short range collisions between the electrons and ions within the capillary. The reduction is neglected in the case of a low density plasma because the collision frequency of electrons and ions is insignificant; however the probability greatly increases in a high density plasma for electrons and ions to collide. To compensate for the conductivity loss, a heuristic method developed by Zollweg and Lieberman was used to replace the Debye shielding parameter in the Spitzer expression for conductivity.

The next result of a non-ideal plasma is that the electrons once considered to be free electrons in the plasma are no longer free, but still remain weakly bonded to the ions. However, there is an effective reduction in the ionization potential that is associated with each species in the plasma because less energy is required to remove an electron to a weakly bound state rather than a completely free state. The increase of collisions will also contribute to the internal energy of the plasma and change the pressure as a function of temperature and density because the electric field produced

by the Coulomb interaction, or collision frequency, is negative, the resulting pressure is less than that of what it would have been from the ideal case. Yet in both cases for the internal energy, and pressure, the difference is still very small and can be neglected, but it is important that the reduction in ionization not be neglected as it is a key variable for calculating conductivity.

The model is assumed to be one dimensional, meaning that all flow variables, or variables acting in the radial direction, are assumed to be constant across the cross section of the capillary with the exception being near the walls, which will be referred to henceforth as the boundary region. We are also assuming the plasma in the model to consist of a homogeneous mixture of carbon and hydrogen ions and neutrals, which is a result of dissociated polyethylene during the ablation process, where most carbon elements are doubly ionized. Both the magnetohydrodynmics and turbulent effects are neglected as well since the magnetic pressures are relatively small compared to the hydrostatic pressure.

3.3) Equations of State

In the previous section concerning the details of ablation, a brief derivation was shown on how to obtain the deposition rate. However concerning the details and equations outlined by Powell and Zielinski, the true ablation rate, which considers length, is derived and then used in their calculations, and can be found in equation 21.

$$\Gamma = \frac{2\rho_b \Delta q}{r_b(P_b + \rho_b E_b)}$$ Equation 21

In equation 21 subscript *b* denotes the variable is very near to the boundary layer, ρ_b is given to be the density of polyethylene, Δq is the heat flux generated by the discharged plasma, r_b is the capillary radius, P_b is the resulting pressure generated in the capillary, and E_b is the specific internal energy of the plasma. It is assumed these values are the averaged over time, and that the heat flux in the capillary is neglected in the longitudinal direction because the length of the capillary is much greater than the radius. The heat flux directed into the polyethylene in the longitudinal direction is also neglected due to the low thermal conductivity of polyethylene. Finally it is assumed the heat flux radiated outward from the capillary is a standard blackbody radiation giving us equation 22 for the heat flux, where σ_S is Stefan-Boltzmann's constant, and *T* is the temperature.

$$\Delta q = \sigma_S T_b^4$$ Equation 22

Pressure, *P*, is determined by assuming the law of partial pressures which will give the following equation 23, where *k* is Boltzmann's constant, n_C and n_H are the number densities of heavy particles for carbon and hydrogen, and x_{ja} is the ratio of heavy particles for the species *a,* where *j* is ionization number, or the ionization factor.

$$P = n_C(1 + x_{1C} + 2x_{2C})kT + n_H(1 + x_{1H})kT$$ Equation 23

To determine the number densities of carbon and hydrogen, a relationship is derived from the density of polyethylene, ρ, and molecular masses of carbon and hydrogen, m_C and m_H where r_0 is the ratio of hydrogen to carbon molecules in a homogeneous mixture of polyethylene, which is two.

$$n_C = \frac{\rho}{m_C + r_0 m_H} \qquad \text{Equation 24}$$

To determine the ion concentration, an equation has been derived from the Saha equations.

$$x_{2a} = K_{2a} x_{1a} = \frac{K_{1a} K_{2a}}{1 + K_{1a} + K_{1a} K_{2a}} \qquad \text{Equation 25}$$

where the ionization function K_{ja} is as follows

$$K_{ja} = \frac{2}{n_e} \frac{Z_{ja}}{Z_{ja-1}} \left(\frac{2\pi m_e kT}{h^2} \right)^{3/2} exp\left[-\left(I_{ja} - \Delta I_{ja} \right) / kT \right] \qquad \text{Equation 26}$$

where n_e is the electron density, Z_{ja} is the electronic partition function, m_e is the mass of an electron, h is Planck's constant, I_{ja} is the ionization potential, and ΔI_{ja} is the reduction in ionization potential due to non-ideality of the plasma. A model for ionization reduction was proposed by Ebeling and Sandig and is given to be as follows where ϵ_0 is the permittivity of free space, *e* is the charge of an electron, λ_D is the Debye length, and Λ is the deBroglie wavelength.

$$\Delta I_{ja} = \frac{je^2}{4\pi\epsilon_0(\lambda_D + \Lambda/8)} \qquad \text{Equation 27}$$

To calculate the deBroglie wavelength and Debye length, with both electron and positive-ion shielding accounted for, the expressions are as follows

$$\Lambda = \frac{h}{(2\pi m_e kT)^{1/2}} \qquad \text{Equation 28}$$

$$\lambda_D = \left[\frac{\epsilon_0 kT}{n_e e^2(1+Z)}\right]^{1/2} \qquad \text{Equation 29}$$

The electron density and effective charge of an ion, *Z,* are also as follows

$$n_e = n_{1H} + n_{1C} + 2n_{2C} \qquad \text{Equation 30}$$

$$Z = \frac{n_C x_{1C} + 4n_C x_{2C} + n_H x_{1H}}{n_C x_{1C} + 2n_C x_{2C} + n_H x_{1H}} \qquad \text{Equation 31}$$

The electronic partition function, Z_{ja}, is determined by the energy levels, U_{jai}, and appropriate degeneracy factor, g_{jai}, for this level, where subscript *j* once again denotes the ionization number and *i* is the electronic state.

$$Z_{ja} = \sum_i g_{jai} exp\left(-U_{jai}/kT\right) \qquad \text{Equation 32}$$

The values of energy levels and degeneracy factors for carbon and hydrogen have been tabulated and are shown on table 1.

Table 3-1 Degeneracy Factors and Energy Levels

	Carbon						Hydrogen	
	$I_{1C} = 11.26\ ev$ $j = 0$		$I_{2C} = 24.38\ ev$ $j = 1$		$I_{3C} = 47.86\ ev$ $j = 2$		$I_{1H} = 13.60\ ev$ $j = 0$	
i	g_{0Ci}	$U_{0Ci}(ev)$	g_{1Ci}	$U_{1Ci}(ev)$	g_{2Ci}	$U_{2Ci}(ev)$	g_{0Hi}	$U_{0Hi}(ev)$
1	1	0	2	0	1	0	2	0
2	3	0.002	4	0.0079	2	6.5		
3	5	0.0054	12	5.35				
4	5	1.27						
5	1	2.69						
6	5	4.19						
7	9	7.5						
8	3	7.7						
9	15	7.96						
10	3	8.56						
11	15	8.66						
12	3	8.79						
13	9	8.87						

In calculating the internal energy of plasma which includes ablation it becomes necessary to take into account the energy required to vaporize, dissociate, and ionize solid polyethylene, as well as to heat the resulting ablation products to the bulk plasma temperature. Also, though usually negligible, the electronic excitation energy for both neutrals and ions is accounted for. Taking the zero energy level to correspond to an unionized gas at zero degrees, the equation for internal energy is as follows

$$E = \frac{1}{\rho}\left[\frac{3}{2}kTn_C(1 + x_{1C} + 2x_{2C}) + \frac{3}{2}kTn_H(1 + x_{1H}) + (I_{1C} - \Delta I_{1C})n_C x_{1C} + (I_{1H} - \Delta I_{1H})n_H x_{1H} + (I_{1C} + I_{2C} - \Delta I_{1C} - \Delta I_{2C})n_C x_{2C} + \rho E_v + \rho E_D + n_C(1 - x_{1C} - x_{2C})W_{0C} + n_C x_{1C} W_{1C} + n_C x_{2C} W_{2C} + n_H(1 - x_{1H})W_{0H}\right] \quad \text{Equation 33}$$

As mentioned before, the vaporization and dissociation energies, E_V and E_D respectively, for polyethylene are taken into account and given to be 2 kJ/g for the vaporization energy and 80 kJ/g for the dissociation energy. In considering the electronic excitation energy, the specific heats of both the solid and gas are neglected in this form of the internal energy because they are relatively very small at high temperatures. The electronic excitation energies can be found from the partition functions by the following relationship

$$W_{ja} = -kT^2 \frac{\partial Z_{ja}}{\partial T} \qquad \text{Equation 34}$$

Now the plasma's electrical conductivity, σ, can be based upon the standard relationship between electron collisions with ions, v_{ei}, and electron collisions with neutral particles, v_{en}.

$$\sigma = \frac{n_e e^2}{m_e(v_{ei}+v_{en})} \qquad \text{Equation 35}$$

It is assumed that the electron neutral collision frequency, v_{en}, can be added to the overall frequency, v_e, and be written in terms of the scattering cross sections of carbon and hydrogen.

$$v_{en} = v_e[(1 - x_{1C} - x_{2C})n_C A_C + (1 - x_{1H})n_H A_H] \qquad \text{Equation 36}$$

$$v_e = \left(\frac{8kT}{\pi m_e}\right)^{1/2} \qquad \text{Equation 37}$$

In equation 36, $A_C = 30\pi a_0^2$, which is the cross sectional area of a carbon atom, $A_H = 17\pi a_0^2$, which is the cross sectional area of a hydrogen atom, and $a_0 = 5.29 * 10^{-11}$m, which is Bohr's radius.

The Spitzer formula is a common method to consider the non-ideal affects for collision frequencies with ions. For this case, a modified expression replaces the usual Spitzer equation to better compensate for the number of positive ions in the plasma. The modified Spitzer equation is as follows

$$\log \Lambda \rightarrow log(1 + 1.4\Lambda_m^2)^{1/2} \qquad \text{Equation 37}$$

The modified Spitzer term now considers the number density of the positive ions, n_+, and then becomes

$$\Lambda_m = \frac{12}{Ze^2}\left[\frac{\epsilon_0 kT}{n_e e^2} + \left(\frac{3}{4\pi n_+}\right)^{2/3}\right]^{1/2} \qquad \text{Equation 38}$$

$$n_+ = n_C(1 + x_{1C}) + n_H x_{1H} \qquad \text{Equation 39}$$

The resulting Spitzer collision frequency then can be shown as

$$v_{ei} = \frac{38Zn_e e^2 log\left(1+1.4\Lambda_m^2\right)^{1/2}}{\gamma_e m_e T^{3/2}} \qquad \text{Equation 40}$$

where γ_e is a weak function of the ion charge approximately equal to 0.58 when Z = 1, and 0.68 when Z = 2.

Though the previous equations listed are sufficient for basic calculations of plasma flow, initial conditions and boundary conditions are set by solving the following differential equations regarding the variables of density, velocity, internal energy, ablation rate, temperature, and pressure. To begin with initial conditions it is assumed the breech end of the capillary is closed, which means the average velocity of the particles is zero. Another initial condition is the pressure at the capillary exit because the gas is usually coupled to conditions exterior to the capillary. Additional boundary conditions for the temperature are applied when considering the effect of longitudinal heat conduction. The values then for density, velocity, internal energy, ablation rate, temperature, and pressure near the boundaries are assumed, as they are with a typical one-dimensional model. The resulting differential equations are as follows

$$\frac{\partial \rho}{\partial t} + \rho \frac{\partial w}{\partial z} + \frac{\partial \rho}{\partial z} = \dot{\rho}_a \qquad \text{Equation 41}$$

$$\rho \frac{\partial w}{\partial t} + \rho w \frac{\partial w}{\partial z} + w\dot{\rho}_a = -\frac{\partial P}{\partial z} \qquad \text{Equation 42}$$

$$\rho \frac{\partial E}{\partial t} + \rho w \frac{\partial E}{\partial z} + P \frac{\partial w}{\partial z} + \dot{\rho}_a (E - w^2/2) = \frac{J^2}{\sigma} - \frac{2}{r_b} q_{rs} - \frac{\partial q_z}{\partial z} \qquad \text{Equation 43}$$

where $\dot{\rho}_a$ is the rate at which plasma density increases dues to ablation, $w\dot{\rho}_a$ is the drag force acting upon the working gas due to ablated molecules entering the system with no initial velocity, $\dot{\rho}_a E$ takes into account the energy expanded by the plasma to begin ablating the polyethylene, $\dot{\rho}_a w^2/2$

is the effect of dissipating energy when ablated molecules enter the mainstream of the plasma arc with no velocity, and J is the current density. The result produces two non-linear equations, which were solved using a Newton-Raphson method, where $\dot{Q}$is the artificial viscosity of the plasma.

$$\dot{Q} = -\rho \Delta z^2 1.5^2 \left(\frac{\partial w}{\partial z}\right)^2 \qquad for\ \frac{\partial w}{\partial z} < 0 \qquad \text{Equation 44}$$

$$\dot{Q} = 0 \qquad for\ \frac{\partial w}{\partial z} \geq 0 \qquad \text{Equation 45}$$

3.4) Isothermal Modeling

To begin modeling a steady state system, it should first be noted that the temperature through the length of the arc remains somewhat constant as the hydrodynamic processes take place much faster on a time scale compared to the current changes. Because the current changes occur much slower relative to those processes the following assumptions can be made. The first is that the ion concentrations, and conductivity are independent of the position because they are functions more so of temperature than the pressure. The next assumption made is that the kinetic energy of the plasma is neglected because many contributions are made to the internal energy at high temperatures, thus the kinetic energy is relatively small.

Taking the previous differential equations 44, and 45, and integrating from length of zero to z, the governing equations are written in conservation form and have the following algebraic results

$$\rho w = \dot{p}_a z \qquad \text{Equation 46}$$

$$\rho w^2 + P = P_0 \qquad \text{Equation 47}$$

$$\rho w E + P w = J^2 z/\sigma \qquad \text{Equation 48}$$

The boundary conditions solved for previously are applied to the flow rate, *w*, and denoted by the pressure, P_0, at the breech end of the capillary. Substituting now the previous equations with equations mentioned in the previous section, the equation for temperature, *T*, formally becomes the following equation, where it is expressed that energy is dissipated through Joule heating radiated through the walls of the capillary.

$$T = \left(\frac{J^2 r_b}{2\sigma\sigma_S}\right)^{1/4} \qquad \text{Equation 49}$$

The pressure state of equation then becomes

$$P = C_{s0}^2 \rho \qquad \text{Equation 50}$$

where C_{s0} is the ion acoustic speed of the plasma, which is independent of position, and given to be

$$C_{s0} = \left[\frac{(1+x_{1C}+2x_{2C})kT+2(1+x_{1H})kT}{m_C+2m_H}\right]^{1/2} \qquad \text{Equation 51}$$

Substituting further equations from the previous sections for the partial pressure will yield the following equations for plasma density, ρ, and particle flow rate, *w*.

$$\rho = \frac{P}{2C_{s0}^2}\left[1 + (1 - 4\dot{\rho}_a^2 C_{s0}^2/P^2)^{1/2}\right] \quad \text{Equation 52}$$

$$w = \frac{2\dot{\rho}_a C_{s0}^2 z}{P}[1 + (1 - 4\dot{\rho}_a^2 C_{s0}^2/P^2)]^{-1} \quad \text{Equation 53}$$

It should be noted that a solution only exists if the following conditions are met, remembering where *l* is the instantaneous position.

$$P \geq 2l\dot{\rho}_a C_{s0} \quad \text{Equation 54}$$

The previous expressions above are for electrical conductivity and ionization factors which are dependent upon position, thus the value for electron density is averaged over the arc length. In order to keep the assumption made previously stating that conductivity and ionization factors are not position dependent we must replace the electron density with the following equation

$$n_e = \rho \frac{x_{1C}+2x_{2C}+2x_{1H}}{m_C+2m_H} \quad \text{Equation 55}$$

The plasma density then must be averaged over the length of the arc as well for the same reason, and can be shown as

$$< \rho > = \frac{1}{l}\int_0^l \rho dz = \frac{P_0}{2C_{s0}^2}\left\{1 + \frac{1}{2N}\left[(N^2-1)^{1/2} + N^2 \sin^{-1}(1/N)\right]\right\} \quad \text{Equation 56}$$

where $N = P_0/(2l\dot{\rho}_a C_{s0})$.

However the initial conditions listed previously for the isothermal model are insufficient, and a more general model must be used initially until a steady state is reached. For the case of the isothermal model, it was shown that the solution did not exist when the calculated pressure generated a particle velocity faster than that of isothermal speed of sound. Yet in the event in which the particle velocity is equal to the isothermal speed, the flow is choked and the breech and exit pressures must satisfy the following relationship

$$P = P(z = 0) = P(z = l) \qquad \text{Equation 57}$$

But when the system is not ideal, and considered to be non-isothermal, the sound of speed requires an additional boundary condition to solve for. At the instantaneous position, the calculation for the speed of sound becomes

$$C_S = \left(\gamma_{eff} P/\rho\right)^{1/2} \qquad \text{Equation 58}$$

where γ_{eff} is the effective adiabatic coefficient of the plasma and is given by

$$\gamma_{eff} = 1 + P/(\rho E) \qquad \text{Equation 59}$$

Chapter 4

Predictive Modeling with Matlab

From the many previous equations listed, it is possible to now predict the characteristics of plasma. This will lead into predicting the ballistics profile of the projectile as well.

4.1) Predictive Modeling

Along with the technical report, Powell and Zielinski developed a model using FORTRAN to easily calculate many of the previous parameters and equations for both ideal and non-ideal plasmas. The model takes three inputs and would generate the plasma outputs by iterative methods. The method in this particular case is known as the Runge-Kutta method, which is used primarily in the case of temporal discretization for the approximation of solutions to ordinary differential equations (ODE's). Temporal discretization is applied for transient problems where both space and time are crucial in the governing equations. It involves the integration of every term in the ODE over a given time step.

The basic Runge-Kutta refines the methods of the Euler method, in such that it uses the average slope of the tangent over an interval to extrapolate the function to the next point. This results in greater accuracy

over Euler's method, which is based upon the midpoint method. The midpoint method will direct the following tangential line through the midpoint of the slope between the two points of the chosen time step, which is most effective for linear extrapolation. Because we are dealing with current pulses, which is better represented by an exponential equation, the Runge-Kutta is superior in that it uses weighted points to account for nonlinear slopes to extrapolate [31].

The most commonly used form of the Runge-Kutta is the classical forth order model. This version requires four evaluations per time step, per integration. Yet having a higher order solver does not necessarily mean higher accuracy, and the code developed by Powell and Zielinski uses only a second order model.

4.2) FORTRAN Iterative Solver

FORTRAN was one of the most commonly used compilers when the original code was developed because of its ability to compute large amounts of data with relatively little computer memory. The version used by Powell and Zielinski is called F77, which improved the recently introduced, at that time, DO loops from the previous version, thus making iteration processes easier to manage. Also F77 was originally designed to run on a Linux operating system, and created several obstacles in understanding the structure of the code. NetBeans is an integrated development environment

(IDE) which is capable of utilizing many different compilers, and was used for the purposes of the researched discussed in this thesis to run the original developed code.

The capillary discharge code originally was designed to be used with an electrothermal-chemical launcher, rather than a gun code. This means that the code assumes the products inside the capillary are streamed out, through the means of expanding air, along with energy which normally remains inside of the capillary. This also means that the theoretical pressure output of the code, due from plasma formation, is less than what is expected in reality because the excess heat energy behind the projectile is not accounted for. This means error is compounded with each passing time step, however it is sufficient enough to determine the peak values and lower bounds for values like ablation, which are time dependent.

The code has three inputs: the experimental time, current, and pressure. However, to formulate a predictive model, the inputs are limited to simulated time and current, where pressure is excluded as it becomes one of the features of the Matlab model, which will be discussed more in detail in the next section. Also the original code requires estimates for the initial values of the plasma bulk temperature, and electrical conductivity. As with many iterative solvers, these initial values are needed to give a range estimate for the system, to keep the governing functions within the proper

bounds. With each passing iteration the code will become more precise as solved equations narrow into the proper values. Yet at a certain point the iterative solver will become less and less efficient with each number of iterations passed. An example of this, not related to the experiments documented in this work, might be that a solver set to 10 iterations might take 10 seconds to process, and yields an accuracy of 80%, but when set to 100 iterations it could take 30 seconds to process and give 95% accuracy. Then comparing this to the same solver with 10,000 iterations which takes 5,000 seconds to process, and gives an accuracy of 97%. It can be seen that time is the trade-off for the cost of accuracy, and the number of iterations no longer are helpful in their calculations if real time is crucial in solving for these equations. Thus the user must select an appropriate balance between the two.

The process of the iterative solver is that it will take the initial values of the plasma temperature and electrical conductivity to solve for other values of the plasma, such as the number densities of the elements, ionization factors, and ablation rate. These solved values then go back to the beginning of the process to solve for the original guessed values at each unit time step, and the loop repeats itself for as many number of iterations are set for the code.

Also the code acts as a quasi-static solver, meaning that it solves to provide a steady state solution for values at any given time. The assumptions made for a steady state iterative solver are similar as the assumptions made before. The system assumes an adiabatic condition throughout the entire capillary, it is a 1-D system so that all properties are constant down the length of the capillary, the capillary is a cylinder with a cross section that is circular, that energy is transported to the polyethylene liner through means of radiation, and the length of the capillary is much greater than the radius. Friction between the projectile and breech is also not considered, as it is relatively small opposing force to the driving force of the projectile. The same assumption is also made for air drag, and can be made for the same reason.

There is also the non-ideality parameter which is built into the Saha equation, which takes into account the Coulomb interactions, where electrons are not completely free from their ion, yet weakly bonded instead. Finally the magnetohydrodynamics are neglected and the breech is assumed to be not choked. This is to simplify the effects of turbulence within the capillary.

The equations listed in the previous section, from the technical report produced by Powell and Zielinski, are the same equation implemented within the code. However, within the code there are different models which

may be implemented for the electrical conductivity. The user is able to select which model to use, and each will produce slightly different results, but by default, the solver will use the method as given by Zollweg and Leibermann. Other empirical models for electrical conductivity have been created since the release of the original code though, and were considered for the development of the model which will be discussed later.

The output of the FORTRAN compiler delivers multiple text files, which can be read with almost any text editor software. The main file of interest includes the following variables; time, current, voltage, adiabatic coefficient, temperature, pressure, number densities, and more. Through NetBeans IDE it is possible to easily manipulate the outputs, and their forms. This is desired for drafting data into graphing software, which will give a visual representation for multiple variables, or allow comparisons between different shots.

4.3) Matlab Iterative Solver

In the transition and translation of the original code, written in FORTRAN, to Matlab, there were several challenges involved. To begin, as mentioned before, the software for F77 was released in 1977 for Linux based computers. This made finding the correct compiler as well as a user interface very challenging as Linux operating systems are no longer a standard. Fortunately NetBeans, by Oracle, has the capability as an IDE to

install compilers for multiple software languages. The recommended compiler, by NetBeans, is called gcc-fortran by Cygwin, which is a software group who hosts many GNU tools and compilers for Linux applications on Windows operating systems. It is also possible to install open source Linux software, such as the Ubuntu OS, which would run the necessary Linux directives to run the original code, yet is not preferred as a standalone executable has also been developed for Windows operating systems in this work.

Learning the syntax of FORTRAN also proved to be very challenging as many of the commands in FORTRAN do not exist in Matlab. For example, the GOTO statement in FORTRAN must be replace by a series of if statements. Much of the learning curve associated for learning FORTRAN programming was overcome through Borse's book "*FORTRAN 77 and Numerical Methods for Engineers"*, published March of 1991, where the syntax is broken down into manageable portions to better learn and understand. Most of what Borse wrote was tailored towards topics in numerical methods, especially matrix equations, curve-fitting, and differential equations, which is ideal for the code developed by Powell and Zielinski. Though syntax was an issue, the logic was still the same as to many software suites used today. Variables must be defined, and are still called upon, mathematical operations behave the same, and to generate an output there first must be an input to describe the system.

Commenting within the code was also not a common practice for FORTRAN users. This made deciphering what the code was trying to accomplish much more difficult. This is also another reason why NetBeans was useful, was so that through a method of trial and error there could be understanding of what the code was trying to accomplish. Many comments were added into the Matlab edition of the code for clear understanding of each section.

A minor issue dealt with some of the input files. Along with the FORTRAN code came several files which described the system. One file carried characteristic values specific to polyethylene and the internal energies associated with ionizing carbon and hydrogen. Another file gave the physical specifications of the systems, such as the capillary radius, capillary length, which conductivity model to use, and the number of iterations to be performed in the calculations. Then FORTRAN would call upon the files as needed to gather information. To simplify, the Matlab edition of the code now includes all of those values in one file, from which all variables are defined.

Another major issue encountered while transitioning to Matlab was the issue of nested loops. In the FORTRAN edition of the code, to accomplish the iterative process, DO loops were established once for the iteration cycle, and then nested DO loops were placed for convenience to

efficiently write each equation for each element and its ionization function. When applying the same logic to Matlab, and using the for loop in place of the DO loop, the results are vastly different due to how each software handles previously generated variables in the memory. When beginning a second, third, or more iterations in FORTRAN the variable clears the previous value and then rewrites the new value. FORTRAN does so because it was designed to be utilized on systems with low random access memory (RAM). Matlab will also write over a value if it is defined to do so, but otherwise stores the data because newer systems are much more capable in terms of RAM.

The issue arises then when calling equations which use previous values of the iteration. FORTRAN will add two values together, the instantaneous iterative value and the previous iterative value. Then with each passing iteration the code clears the iteration that is two previous of the current iteration so that it, or any future values, will not see values for any other iteration other than the one previously generated. Matlab does not operate in the same fashion for nested loops. Matlab, because it has the RAM capability, will keep each passing value of the iteration and recall it every time the equation is called. As one can see, error quickly compiles and the value reaches an erroneous state.

To overcome the issue of nested loops, more lines of code were added which separated the governing differential equations into multiple sections. One section contained the code which ran the equation for the current iteration. Another section then stored data from the previous iteration, and with the next iteration was rewritten to the correct value. Then a final section of code that was added combined the result of the current iteration and the iteration previous to the current.

4.3.1) Matlab Additions and Improvements

The first addition made to the previous code was eliminating the need to have multiple input files, and reduced it to only one input file, containing time and current values. As mentioned before, many of the files were used to describe the physical aspects of the system, and were easily implemented as part of the code file. The remaining input file was then brought forth from Matlab's importdata command, which is an intelligent method to import data from most structures and file types. For the sake of simplicity, only comma separated value files (.csv), and text files (.txt) with comma delimiters were accounted for in the design of the new code, as cell and array structures begin to change when in a different format, thus making the code worthless as it does not have the ability to process matrices and arrays outside of the ones pre-defined.

The number of iterations is crucial to precision, as well as how long it takes to compute the code. Because the user may desire one trade-off more than another, Matlab has been programmed to ask the user at the beginning of each run how many iterations it should perform. This will ensure that the most efficient balance between time and precision has been defined by the user. However, as mentioned before, having a high number of iterations does not necessarily result in much greater precision, and with current technology it is possible to have both precision with short calculation times. It should be noted though that certain errors will occur at high iterations. This is because of the method being implemented by the Runge-Kutta, which uses second order differential equations, relies on the set bounds given beforehand to keep values within an acceptable range. The error occurs specifically when noise enters into the simulation, which has no bounds, and thus is free to compound error exponentially with each passing iteration.

For the ideal case, the current pulse used for the system input does not contain any noise with the signal, but rather a pure signal is produced, and the value at steady state is equal to zero. However noise is inevitable in real world measurements, and Pearson coils, which are commonly used in current pulse measurements, are prone to noise at steady state measurements. This is because the Pearson coil was designed by the to operate on Faraday's Law, which states that when a magnetic field is

applied perpendicular to a component the resulting charge accumulates on the surface of the component. In order for the magnetic field to be perpendicular, it must curve in a circular fashion around the wire carrying current. If any portion of the magnetic field aligns perpendicularly to the direction in which the current travels it will not produce the Hall Effect, but rather a Lorentz force, which was described earlier. The differential of the current is then measured, because the magnetic field is a result of a time varying electric field as stated in Maxwell's equations. When there is no time varying current, or no current at all, the magnetic field will either not exist and the readings given from the Pearson coil are a result of noise.

To compensate for this error, Matlab allows for noise filters to be added. Yet for simplicity, it is assumed that the input file does not contain noise. As the code is a predictive model now and predicts the plasma parameters, rather than an evaluation model as originally designed to calculate plasma parameters, we can assume the data input is based upon simulation with no noise and not experimental data. It is fair to make this assumption because even in experimental results with noise, the peak current value is still determined to be very accurate. This is important because the peak pressure value is strongly correlated to the peak current value, and the peak pressure is used to calculate ballistic equations, which will be discussed in detail later.

Since the release of the original code, new empirical models have been developed for plasma as well. Many researchers are in agreement that plasma conductivity is strongly related to the electron-ion collision frequency, but how to calculate the collision frequency is often a topic of debate. Rather than using one specific equation, and risk large error, it was decided to take several models and take the average so that a weighted evaluation could be taken. The original models were given by Kurilenkov and Valuev, Zollweg and Liebermann, and Hahn, Mason, and Smith, with the default choice being Zollweg and Liebermann's model. In total 3 more models were taken into account. Gurnett's model is similar to Zollweg and Liebermann's but instead Gurnett neglected the electron-neutral collision frequency and has the following form [32]

$$\sigma = \frac{n_e e^2}{m_e \nu_{ei}} \qquad \text{Equation 60}$$

Liebermann produced a model alone, and has a strong dependency upon the plasma bulk temperature and Spitzer logarithm, where the collision frequency is built into the equation, as given before. It has the following form [33]

$$\sigma = \frac{0.019T^2}{\Lambda} \qquad \text{Equation 61}$$

Piel developed his model with the claim that is similar Liebermann's standalone model, but gave more credit to the plasma density. Piel's equation is given to be [34]

$$\sigma = \frac{(4\pi\epsilon_0)^2 (kT)^{3/2}}{\Lambda e^2 m_e^{1/2}} \qquad \text{Equation 62}$$

Each conductivity model is within an acceptable range, and can better be seen in figure 23 and figure 24.

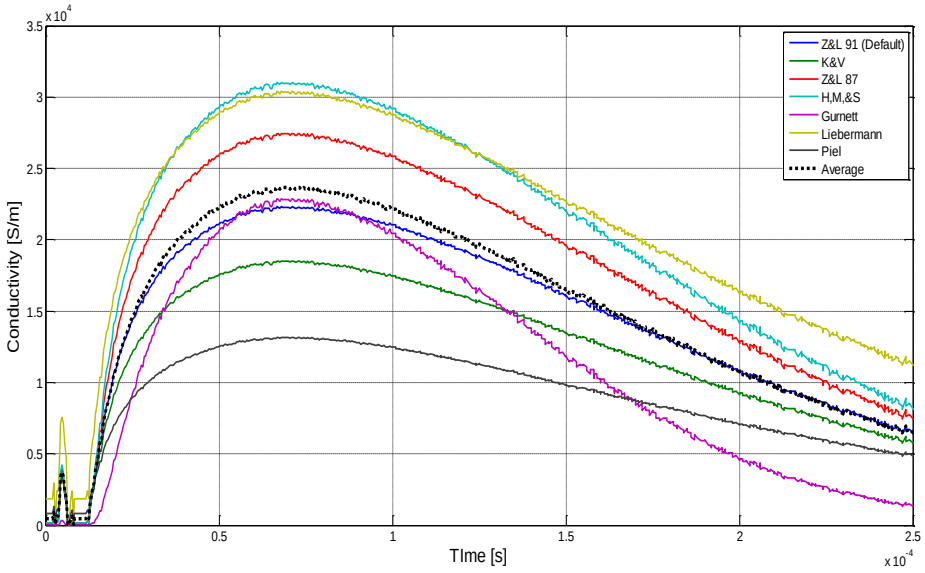

Figure 4-1 Conductivity Options

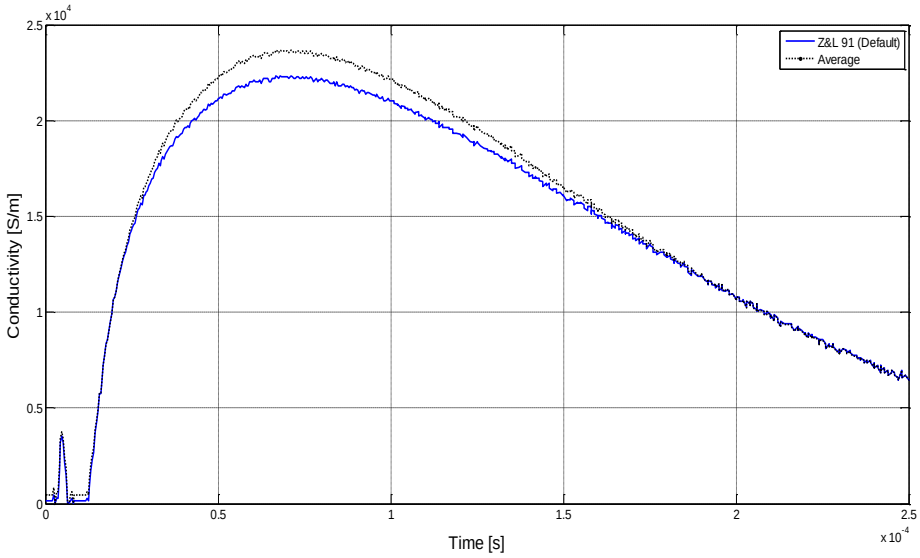

Figure 4-2 Average Conductivity Model

The next adjustment to generate a predictive model took place in the averaging function. In order to establish a model independent of an experimental pressure, the N parameter used in the integral for averaging was adjusted. Originally the N parameter was used as another method to keep the system calculations within the proper bounds. If by chance any value tried to stray into error, the N parameter would act as a negative feedback block, and keep the error from growing too much. This was done through the integral for averaging which was applied in the resistivity equation. As the resistivity would try to grow in error, the N parameter would balance it by being multiplied to the resistivity. By default the value for the N parameter is one, but as error grew the N parameter would decrease to zero, thus resistivity was forced to stay within the bounds.

For the Matlab code, it was assumed that the N parameter is always equal to one. By making this assumption we are able to eliminate the need for an experimental pressure input, which is important because one objective of this study is to predict the system pressure. This assumption can be made because the governing equations for plasma characteristics rely heavily upon the current pulse given as the input. As long as there are no discrepancies with the simulated current pulse, the assumption made will hold true.

A ballistics model has also been added into the Matlab code as well. Though it will be discussed in greater detail later, it is derived from the partial pressure equation as given by Powell and Zielinski. The ballistics equation can predict the output velocity of a given projectile from the predicted pressure. This can be done because it is known that the pressure is dependent upon the ablated material within the chamber, as well as the bulk plasma temperature, which are both calculated and known.

Discussed in the previous section were different models for ablation. Another addition the Matlab code includes is Rui Li's and Xingwin Li's model-L for ablation, which is based upon the enthalpy of polyethylene. This model was added because it is solely dependent upon the bulk plasma temperature, and also in terms of computation speed is less of a load in the calculations than the model presented by Powell and Zielinski. The model

by Powell and Zielinski require that the ablation equation be run through every iteration of the code, and is also dependent upon more variables, such as the internal energy of the plasma and the different partition functions. Then it is clear that Mode-L, which only requires temperature and does not go through the same iterative process, is less of a burden to the computational system. Though minor discrepancies occur, it can be seen in figure 25 that model-L is suitable for calculating the ablated mass of polyethylene.

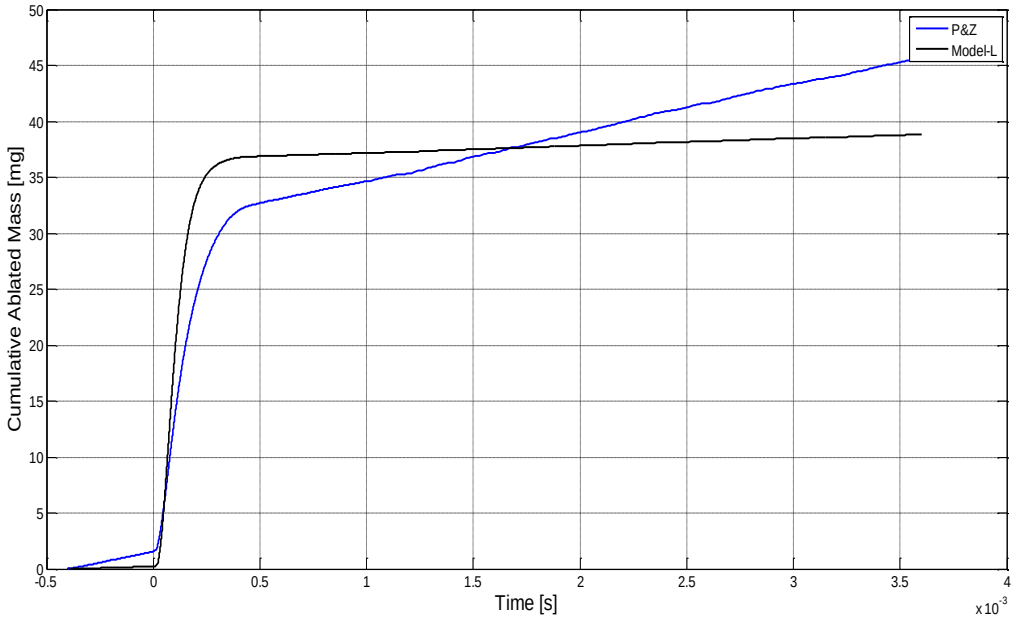

Figure 4-3 Ablation Model Comparison

Finally the last improvement made to the code was that a user-friendly general user interface (GUI) was developed to enable an easy way to use the Matlab code. Before, in the development of the original code, because

the system it was designed for was Linux, it cannot run as an executable in any Windows operating systems. Thus the code became of no worth to many, unless decided to and were able to find a suitable FORTRAN compiler which would function in Windows, but as seen before it takes several more steps to run the code. Also the executable file ran all calculation in the background as a script, where it could not be seen to the user what was taking place, or if there was any error. An executable file for Windows was also developed, and eliminates the need to take extra steps to run a FORTRAN compiler, and will be discussed in more detail later. The outline of the GUI can be seen below in figure 26.

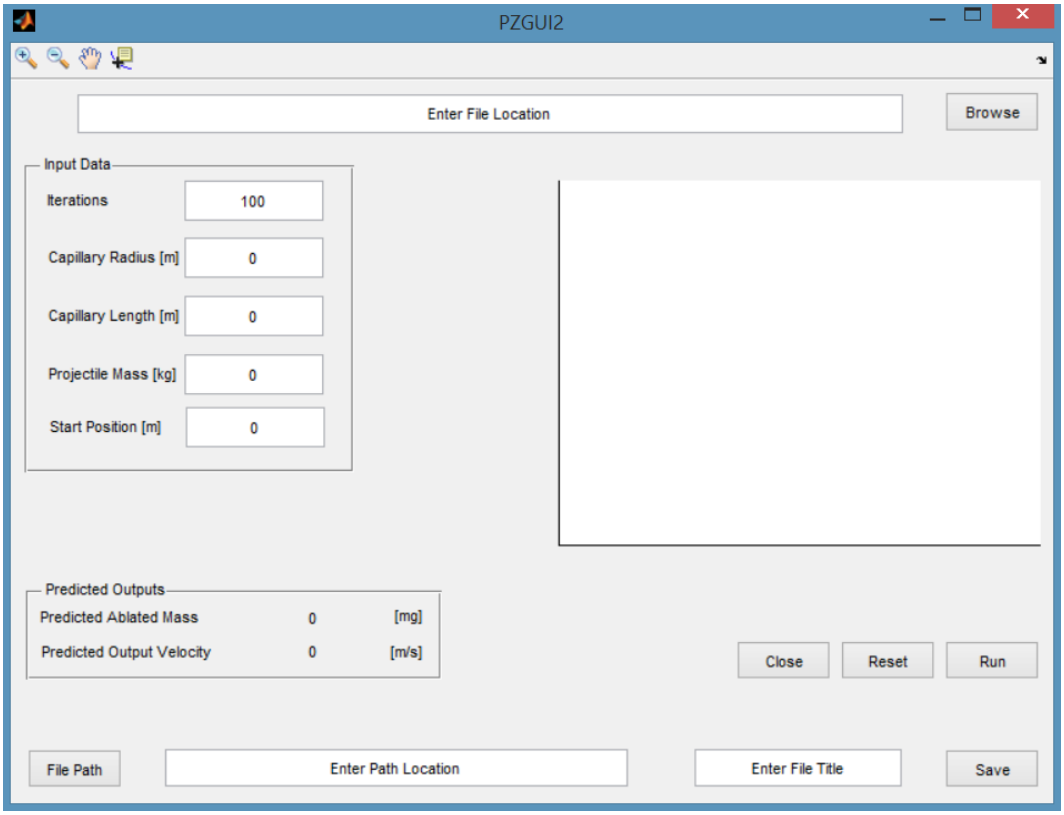

Figure 4-4 Matlab GUI

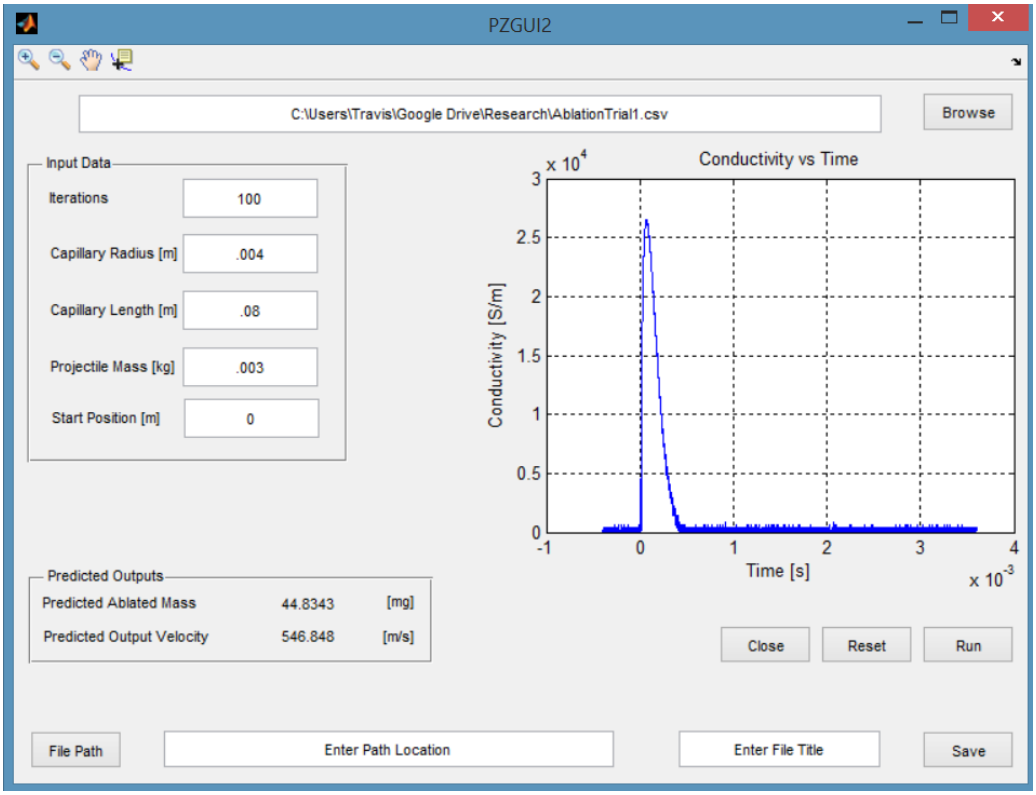

Figure 4-5 Matlab GUI Execution

The GUI allows the user to easily change which files are used for input by browsing through selected folders, whereas the old executable required that all input files were kept together in the same folder. This then allows the user to quickly run and analyze several sets of data in an efficient manner. As seen above in figure 27, there is a built in graph function which shows the plasma conductivity over the time of discharge. This serves two purposes; the first purpose is to show the user that the input data used is functional with the Matlab code, and the second is to give the user a quick idea as to how accurate their data is.

4.3.2) A Brief Comparison of Models

When looking at the different models side-by-side the basic functionality remains the same. Both models use the same governing equations to determine the characteristics of plasma, therefore they replicate many of the same results. Differences can be noticed on a microscopic level however, as each compiler behaves differently for rounding variables. This is due to the set floating point number, which is specified by the programmers responsible for creating the compilers. As Matlab is the newer software, it will be slightly more accurate due to its ability to keep track of more significant values. However these rounding errors seen in FORTRAN are negligible because of how small the compounded error is. In fact, as seen in figure 28 the two sets of code look near identical.

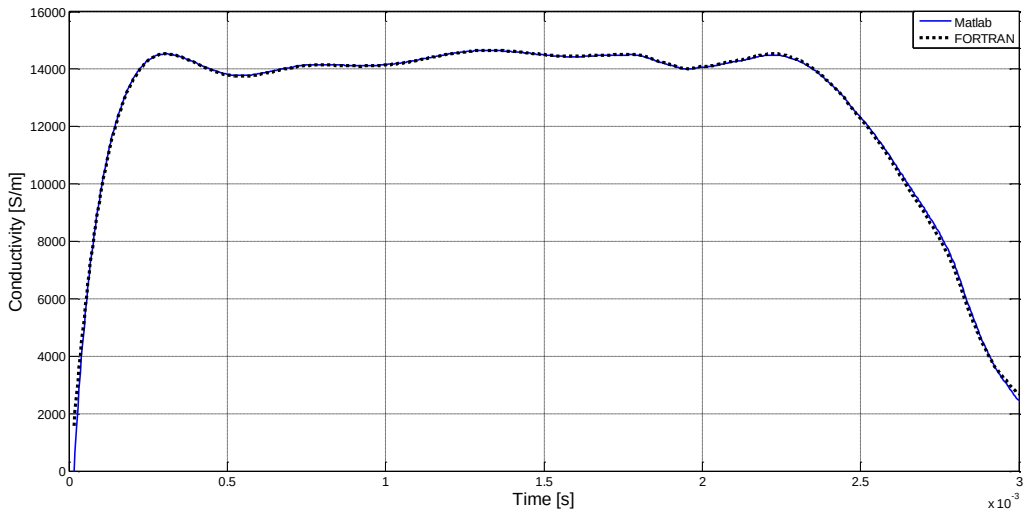

Figure 4-6 Model Comparison: FORTRAN and Matlab

As far as computational time is concerned, both programs take relatively the same amount of time. Without getting into the details, by speculation FORTRAN would have the edge, as it was designed to be a lightweight system. Yet both programs run at an acceptable speed, and there is very little time difference, if any at all. So then it can be said that time is mainly a factor on the number of iterations performed for each run in each program.

The main benefit of using the script generated by Matlab, though stated in the previous section, is much easier to navigate; especially for users with little to no programming experience. The GUI alone has significant value in that the common user can intuitively upload the file they need evaluated in a relatively short amount of time. The updated methods to uploading the input data is also of much benefit because more data is able to be processed with less amount of time between each run. With the files all in one file, and built into the code, the user doesn't bother going into each individual file checking to make sure that the system parameters are correct, but rather the system parameters are made visible within the GUI and are easily able to be changed at the desire of the user. Finally the Matlab code has been designed to run on all Windows OS, which is the standard during the time the updated code was developed.

Chapter 5

Ballistic Profiling of an Electrothermal Launcher

Based upon the previous prediction, the output velocity of the projectile is now of interest. The predicted pressure output will play a key role in determining the exit velocity.

5.1) Ballistic Modelling

As mentioned in the previous section, the ballistics model is a new addition to the previously developed code. It allows for the output velocity of the projectile to be predicted at the end of the breech, where free flight begins. It will be shown in this section how pressure, generated by the ablating polyethylene liner, will be the primary force acting upon the projectile.

The projectile of an electrothermal launcher has some similarities to the conventional launcher, specifically a bullet propelled by the combustion of gunpowder. When the gunpowder in the bullet casing is first ignited by the primer, the individual grains of gunpowder are part of an avalanche type effect, where the first grain, when ignited, generates an exothermic chemical reaction, which then ignites the grains in the surrounding proximity, and the process repeats so on until each grain has been ignited. Another product of the exothermic reaction is the expansion of air; the newly

combusted particles are filled with energy and move rapidly in the enclosed volume, bouncing off of the casing walls, and each other, trying to reach a state of equilibrium. This then becomes the driving force behind the bullet, as the only path allowed for the expanding air to escape, and go back to the lower energy state of equilibrium, is down through the exit of the barrel.

It can be seen then that the resulting pressure will resemble that of a current pulse. This is because the gunpowder will not and cannot continuously generate energy, but only exert energy during the combustion process, which happens on the time scale of hundreds of micro to milliseconds. Then the pressure, after reaching its peak value, will begin to decrease rapidly until a state of equilibrium is reached. This is for two reasons; the first, as mentioned, was that there is no more instantaneous exothermic energy being generated, and the second is that the volume is constantly increasing while the projectile moves down the barrel. Then it can be assumed that the value of interest is only the peak pressure point, because after the peak there is little work being done on the bullet.

Railguns, as mentioned before, are superior in their ability to achieve higher exit velocities. Because of Lorentz's Law, the force moving the projectile in a railgun is created by the moving current of a pulse forming network, the ability to vary the force is possible by varying the current. Therefore if multiple power supplies are cascaded to keep a large peak

current for an extended period of time, approximately around hundreds of milliseconds, then the force acting upon the projectile behaves similarly, in that the period of time in which the force acting upon the projectile is increased.

The current, which generates the Lorentz force, travels the length of the barrel up to the instantaneous position of the projectile. Because railguns have the ability to apply a constant force throughout the entire length of the barrel, rather than the impulse seen in a conventional launcher, exit velocities may easily reach speeds in excess of that of the speed of sound.

In the case of an electrothermal launcher, the expansion of air is due to the ablated wall liner as described in a previous section. In summary, the capillary discharge happens after a large voltage is applied to the terminals until voltage breakdown occurs. At voltage breakdown electrons begin to bridge the gap between anode and cathode, which generates an initial stream of plasma. The plasma then ablates the polyethylene liner through the heat flux generated, which dissociates carbon and hydrogen atoms from there bonds. Some of the newly released particles then contribute even more to the plasma by ionizing, and releasing one or two electrons from their valence shell.

The ablated particles are then responsible for the expansion of air, as they are the “excited”, or energized particles. As more and more particles flood into the capillary, the pressure will rapidly increase, and once again, as like the conventional launcher, the air seeks to reach a state of equilibrium. The only means in which the air may reach equilibrium though is still by forcing the projectile forward, through to the exit of the breech.

5.2) Predicting Exit Velocity

To begin to predict the exit velocity of a projectile launched by an electrothermal launcher, the law of partial pressures is used. From the previous section it was seen that the pressure generated in the capillary is given to be as follows

$$P = n_C(1 + x_{1C} + 2x_{2C})kT + n_H(1 + x_{1H})kT \qquad \text{Equation 63}$$

With the pressure now calculated, the next step is to find the acceleration of the projectile. This can be done with the following relationships. In the first equation, pressure is equal to the force, F, distributed of an area, A.

$$P = \frac{F}{A} \qquad \text{Equation 64}$$

The force is known to be the product of the projectile mass, m, and the projectile acceleration, a.

$$F = m \cdot a \qquad \text{Equation 65}$$

Now the equation is rearranged to solve for the projectile acceleration in terms of the pressure and can be shown as

$$a = \frac{PA}{m} \qquad \text{Equation 66}$$

Then taking the integral of the acceleration, with respect to time, we can find the relative velocity, v, at which the projectile will travel.

$$v = \int_0^t a\, dt \qquad \text{Equation 67}$$

But because the system does not continually act upon the projectile, as mentioned before, a new system of equations must be implemented to account for other factors of the plasma and pressure. In Jerry Parker's report for a plasma driven pre-injector, he outlined a method in which to find the exit velocity. The equation described is based upon the pressure energy, and adiabatic laws. The exit velocity predicted can be given as the following

$$v = \left[\frac{2P_i a^2 (x_i + x_r)}{(\gamma - 1)m}\right]^{1/2} \left[1 - \left(\frac{x_i + x_r}{x_f + x_r}\right)^{\gamma - 1}\right]^{1/2} \qquad \text{Equation 68}$$

where P_i is the peak pressure, x_i is the initial position of the projectile relative to where the capillary and breech meet, x_r is the reference position, or instantaneous position, x_f is the final position of the projectile before free flight begins, or the length of the breech, and γ is the adiabatic coefficient which was given earlier.

To calculate the reference position an assumption is made, based upon the initial equations given in this section. The instantaneous position is assumed to be equal to the integral of the velocity, with respect to time.

$$x_r = \int_0^t v\, dt \qquad \text{Equation 69}$$

These equations were all implemented into the previously described GUI, as part of the updated features. It can easily be implanted, as the length of the breech and the initial position are able to be changed to the user's desire before each launch simulation.

Chapter 6

Conclusion and Summary

Coming forth from conventional launchers and electromagnetic launchers, electrothermal launchers are unique systems which possess many of the benefits of both the conventional and electromagnetic launcher. The main benefits of an electrothermal launcher are that they are safe, predictable, and can be adjusted.

Electrothermal launchers are considered to be safer than a conventional launcher for a number of reasons. The gunpowder used in a conventional launcher has no protection other than the metal casing in which it is enclosed into. This makes the gunpowder prone to the surrounding environment, and a hazard in harsh and extreme conditions. Electrothermal launchers use energy stored in a readily available capacitor bank. The capacitors, when they are not in use, will remain discharged, thus presenting absolutely no danger in the event of an emergency. When the capacitors do need to be charged though, the charging process may take up to ten seconds, depending on the size of the capacitor bank and power supply, and be readily available for discharge.

The reliability and predictability are major benefits as well. As mentioned, conventional launchers store gunpowder in metallic casing. Along with the safety concern, this produces a reliability issue. Gunpowder

is very susceptible to any moisture in the air, and will not properly ignite if dampened. Thus storing gunpowder in a dry environment becomes an issue. Though there are many electrical connections in the electrothermal setup, they are very reliable, if properly installed. The electrical energy stored in the capacitor bank is drawn from the instantaneous energy of a generator, being stored to be almost immediately used.

The process of an electrothermal launch has high repeatability rates as well. Where gunpowder is made of many different grain sizes, it becomes somewhat of a guess to predict how the projectile will perform. As the surface are of the gunpowder increases, the burn rate will increase. But to manufacture grains in consistent in size is near impossible, and the burn rate will vary from bullet to bullet. Because the heat flux ablating the polyethylene is directly proportional to the current, not only is it possible to repeat a shot with very close results, but it can now be seen that the performance is not limited to a single type of shot.

The pulse forming network allows the current used in the capillary discharge to have an extended duration with a low peak, or pulse at a high peak. From the expressions given before, it can be seen that control over the current gives control over the heat flux, which is advantageous as it is directly related to the ablated mass, and thus the pressure. Now it is

possible to predict the exit velocity, as the pressure function is given by a reliable equation.

The PFN was determined by the parameters define by a series RLC circuit. To set the current to a desired value, the system voltage was taken to be the sum of the following: the inductance multiplied by the time differential of the current, the voltage across the resistive elements, and the stored charge over the capacitance. To vary the voltage, any of those elements may be changed. Usually the inductors are taken out of series, which presents another concern.

The dampening of the system is critical. In order to prevent any damage to the equipment, the system must either be critically damped or over damped so that there is no current returning in the reverse path. If the system is underdamped, then the current will ring in an oscillatory fashion. The negative peaks of the oscillation are what cause reverse current flow, and forces energy through the power supply, which will cause damage to different parts.

The current becomes a free flowing plasma in the capillary when a large enough voltage is applied between the anode and cathode, then voltage breakdown occurs. The capillary, also called the pre-injector, is a steel cylinder, which allows for a return path to ground for the electric flow, while containing the heat flux in a safe manner.

The heat flux then ablates the outer layer of the polyethylene liner, releasing carbon and hydrogen particles into the capillary, flooding the vacuumed chamber with expanding particles. These energized particles now produce work in the capillary by pushing forward the projectile through the exit of the breech.

Though ablation is dependent upon mainly the heat flux, other factors were crucial for investigating this phenomena. The size of the capillary, specifically the cross sectional area, was used in calculating the rate of ablated mass. Pressure was also a key element, because as the pressure increased, the state in which the polyethylene would dissociate elements would also change.

Different models have been proposed in recent years for ablation as well. Model-L takes into account the ablation enthalpy of polyethylene and uses only the bulk plasma temperature for calculating the ablated mass. Also studies have been conducted to better understand the hydrodynamic layer and Knudson layer of the plasma. The plasma behaves differently as it approaches the outer bounds, and enters into a turbulent state, thus becoming more unpredictable. To estimate ablation through the Knudson layer, a two layer kinetic model was created, which accounts for the temperature of the bulk plasma, and the temperature at the outer boundaries of the plasma.

Calculating the other characteristics of plasma came from a detailed report given by Powell and Zielinski, where it was shown how the heat flux is generated, and its relationship to pressure. Furthermore, the electrical conductivity of the plasma relied on the number of carbon and hydrogen elements which were ionized, by dissociation of the heat flux. But the electrical conductivity of plasma is still not very well understood, and many models have been empirically driven.

In order to establish a predictive model, the electrical conductivity was crucial in the calculations. The method used to calculate the characteristics of plasma was by means of an iterative solver. Because the bounds of plasma were set by previous conditions, an iterative solver can predict many different characteristics of plasma based upon the equations outlined in the BRL, as long as the current profile used as the input was also within the bounds. The conductivity model used was not one individual model, but rather an average of multiple models to help eliminate whatever error might be contained in the individual model.

Originally solved by means of a FORTRAN compiler, the model derived by Powell and Zielinski was updated to run within Matlab. Along with the original script, the Matlab code contained some improvements. Some minor improvements include the layout of the code, made within a GUI for ease of use, and the ability to quickly handle data. However the

biggest improvement to the original script was the addition of the ballistics calculations. The ability to forecast the output velocity of a projectile was outlined by Jerry Parker, and was implemented into the GUI. Finally the GUI was created to be an executable file which would run on any Windows PC.

Finally a comparison, shown on table 2, gives an idea of how close the simulated data is to that of the recorded experimental data. It can be seen that there are some discrepancies in the ablated mass, and the exit velocity for the experimental data. This is because the measured ablated mass was measured on less sensitive scale, and the Photonic Doppler Velocimetery (PDV) method is prone to noise.

Table 6-1 Comparison of Data

	Experimental Data			Simulated Data		
Shot Fired	Current (kA)	Mass Loss (g)	Exit Velocity (m/s)	Current (kA)	Mass Loss (g)	Exit Velocity (m/s)
1	37.38	0.0501	623	37.28	0.04997	602
2	37.43	0.0274	627	37.44	0.0457	611
3	37.98	0.0476	563	37.44	0.0739	604
4	37.86	0.0304	660	37.76	0.04967	615
5	37.39	0.0477	610	37.44	0.04293	604

6.1) Future Works

There are a number of items to be considered for the future work of this project. The biggest consideration to make would be the evolving of electrothermal launchers into the electrothermal-chemical launcher regime. Not much is known now how chemicals exposed to plasma discharge will behave. Certain combinations of chemicals are being added to vary the heat flux, and generate a larger pressure peak, but it is still in the very early stages of development.

The power supplies used for the PFN's are vastly oversized still, and much research is being done to develop more energy dense super capacitors. To reduce the size of the capacitor bank would mean making a device, such as an electrothermal launcher, much more portable, and give it more applicable uses.

Though the ballistics model is seemingly accurate when compared to experimental data, the specific heat ratios are somewhat of a mystery. The adiabatic coefficient plays a key role in determining the exit velocity, as it describes the conditions of the air within the capillary. The capillary code should also be updated to consider an open system.

Last of all, the model could also benefit by updating the ablation model, as there is much research to be done within the kinetic layer and Knudson layer. The magnetohydrodynamics are, as of now, ignored

because there is no easy way to implement them, plus they are not very well understood.

References

[1] - Wetz, David A., Francis Stefani, Jerald V. Parker, and Ian R. McNab. "Advancements in the Development of a Plasma-Driven Electromagnetic Launcher." *IEEE TRANSACTIONS ON MAGNETICS* 45.1 (2009): 495-500. *IEEE Xplore*. Web. 18 Aug. 2012.

[2] - "Sling (weapon)." *Wikipedia*. Wikimedia Foundation, n.d. Web. 2 Oct. 2013.

[3] - Harrison, Chris. "The Sling in Medieval Europe." *The Bulletin of Primitive Technology* 31 (2006): n. pag. *Chris Harrison*. Web. 2 Oct. 2013.

[4] - "Stone-Age arrows found". University of Johannesburg. Retrieved 24 August 2012.

[5] - "Bows." Weapons: An International Encyclopedia from 5000 B.C. to 2000 A.D.New York: St. Martin's, 1990. 94-105. Print.

[6] - Buehr, Walter. Firearms. New York: Crowell, 1967. Print.

[7] - "Electricity." *Wikipedia*. Wikimedia Foundation, n.d. Web. 2 Oct. 2013.

[8] - Bellis, Mary. "Thomas Edison Improves The Stock Ticker." *About.com Inventors*. About.com, n.d. Web. 2 Oct. 2013.

[9] - "How Capacitors Work." *HowStuffWorks*. N.p., n.d. Web. 2 Oct. 2013.

[10] - McNab, Ian R. "Early Electric Gun Research." *IEEE TRANSACTIONS ON MAGNETICS* 35.1 (1999): 250-61. *IEEE Xplore*. Web. 2 Oct. 2013.

[11] - Egeland, Alv. "Birkeland's Electromagnetic Gun: A Historical Review." *IEEE TRANSACTIONS ON PLASMA SCIENCE*17.2 (1989): 73-82. *IEEE Xplore*. Web. 2 Oct. 2013.

[12] - "Air Gun." *Wikipedia*. Wikimedia Foundation, n.d. Web. 2 Oct. 2013.

[13] - "Light Gas Gun." *Wikipedia*. Wikimedia Foundation, n.d. Web. 2 Oct. 2013.

[14] - Watt, Trevor, Francis Stefani, Mark Crawford, Hans Mark, and Jerald Parker. "Investigation of Damage to Solid-Armature Railguns at Startup." *IEEE TRANSACTIONS ON MAGNETICS* 43.1 (2007): 214-18. *IEEE Xplore*. Web. 2 Oct. 2013.

[15] - Stafani, F., I. McNab, J. Parker, M. Alonzo, and T. Klatt. "A Plasma Railgun Experiment Addressing Launch-to-Space Issues." *IEEE TRANSACTIONS ON MAGNETICS* 43.1 (2007): 194-97. *IEEE Xplore*. Web. 2 Oct. 2013.

[16] - "Naval Railguns." *IEEE TRANSACTIONS ON MAGNETICS* 43.1 (2007): 463-68. *IEEE Xplore*. Web. 2 Oct. 2013.

[17] - Witherspoon, F. D., R. Bomgardner, A. Case, S. Messer, L. Wu, and HyperV Technologies Corp. "Minirailgun Accelerator for Plasma Liner Driven HEDP and Magneto-inertial Fusion Experiments." (n.d.): n. pag. *IEEE Xplore*. Web. 3.

[18] - Hilmes, Rolf. "Military Technology." *Aspects of Future MBT (Main Battle Tank) Conception* 23.6 (1999): 72-76. Web. 2 Oct. 2013.

[19] - D. Berry. “A Primer (not pr-eye-mer) On Guns”, IAT-T-0392: Austin, Texas: Institute for Advanced Technology. 1992.

[20] - Motes III, Doyle T. "A Study of Gas Dynamics and Properties of a Capacitively Driven Electrothermal Launcher." Thesis. The University of Texas at Austin, 2008. The University of Texas at Austin. Web. 2 Oct. 2013.

[21] - McNab, Ian. "A Research Program to Study Airborne Launch to Space." *IEEE TRANSACTIONS ON MAGNETICS*43.1 (2007): 486-90. Web. 2 Oct. 2013.

[22] - Reithel, R., J. Blackburn, G. Seay, and S. Skolnick. "The Current Pause in an Exploding Wire." Editorial. *The Library of The University of Texas* n.d.: 19-33. Print.

[23] - Motes III, Doyle T. "A Study of Gas Dynamics and Properties of a Capacitively Driven Electrothermal Launcher." Thesis. The University of Texas at Austin, 2008. The University of Texas at Austin. Web. 2 Oct. 2013.

[24] - NASA. "Ablation." *Dictionary of Technical Terms for Erospace Use* -. N.p., n.d. Web. 2 Oct. 2013.

[25] - Pekker, L., M. Keidar, and J.-L. Cambier. "Effect of Thermal Conductivity on the Knudsen Layer at Ablative Surfaces."*Journal of Applied Physics* 103.3 (2008): 034906. Print.

[26] - Keidar, Michael, Iain D. Boyd, Anthony Williams, and Richard Beyer. "Ablation Study in a Capillary Sustained Discharge."*IEEE Transactions on Magnetics* 43.1 (2007): 308-12. Print.

[27] - Keidar, Michael, and Iain D. Boyd. "Ablation Study in the Capillary Discharge of an Electrothermal Gun." *Journal of Applied Physics* 99.5 (2006): 053301. Print.

[28] - Porwitzky, A.j., M. Keidar, and I.d. Boyd. "Numerical Parametric Study of the Capillary Plasma Source for Electrothermal–Chemical Guns." *IEEE Transactions on Magnetics* 45.1 (2009): 574-77. Print.

[29] - Li, Rui, Xingwen Li, Shenli Jia, and Anthony B. Murphy. "A Two-dimensional Capillary Discharge Model considering the Ablation and Deposition Processes." *Journal of Applied Physics* 110.9 (2011): 093302. Print.

[30] - Li, Rui, Xingwen Li, Shenli Jia, Anthony B. Murphy, and Zongqian Shi. "Study of Different Models of the Wall Ablation Process in Capillary Discharge." *IEEE Transactions on Plasma Science* 38.4 (2010): 1033-041. Print.

[31] - Borse, G. J. "Chapter 10: Iterative Solving Methods." *Instructor's Manual: FORTRAN 77 and Numerical Methods for Engineers, Second Edition*. Boston: PWS-KENT Pub., 1991. N. pag. Print.

[32] - Gurnett, Donald A., and A. Bhattacharjee. *Introduction to Plasma Physics: With Space and Laboratory Applications*. Cambridge, UK: Cambridge UP, 2005. Print.

[33] - Lieberman, M. A., and Allan J. Lichtenberg. *Principles of Plasma Discharges and Materials Processing*. New York: Wiley, 1994. Print.

[34] - Piel, Alexander. *Plasma Physics: An Introduction to Laboratory, Space, and Fusion Plasmas*. Heidelberg: Springer, 2010. Print.

Biographical Information

Travis M. Least was born in Lexington, Kentucky on October 10th, 1989. Having spent most of his life in Flower Mound, Texas, Travis graduated from Flower Mound High School in 2008. He then went on to pursue a bachelor's of science degree in electrical engineering at Texas Christian University. While there he was an active member of Beta Upsilon Chi, and IEEE, and developed interests in electronics and power systems. After graduation, in May of 2012, Travis began work for Dr. Wetz in his pulse powered lab as a graduate research assistant until graduation.